1 Atmospheric Aging Enhances the Ice Nucleation Ability of Biomass-Burning Aerosol

- 2 Lydia G. Jahl¹, Thomas A. Brubaker¹, Michael J. Polen^{1,†}, Leif G. Jahn^{1,‡}, Kerrigan P. Cain^{1,§},
- 3 Bailey B. Bowers¹, William D. Fahy¹, Sara Graves¹, Ryan C. Sullivan^{1,*}
- ¹Center for Atmospheric Particle Studies, Carnegie Mellon University, 5000 Forbes Avenue,
- 5 Pittsburgh, PA 15213, USA.
- [†]Present address: Department of Chemistry, McDaniel College, 2 College Hill, Westminster,
- 7 MD 21157, USA.
- 8 [‡]Present address: Department of Chemical Engineering, University of Texas at Austin, 110
- 9 Inner Campus Drive, Austin, TX 78705, USA.
- [§]Present address: Photovoltaic and Electrochemical Systems Branch, NASA Glenn Research
- 11 Center, 21000 Brookpark Road, Cleveland, OH 44135, USA.

12

- ^{*}Correspondence to: Ryan C. Sullivan, Department of Chemistry & Department of
- Mechanical Engineering, 2111 Doherty Hall, 5000 Forbes Avenue, Carnegie Mellon
- University, Pittsburgh, PA 15213, USA. (412) 268-8462, rsullivan@cmu.edu.

Abstract

Ice nucleating particles (INPs) in biomass-burning aerosol (BBA) that affect cloud glaciation, microphysics, precipitation, and radiative forcing were recently found to be driven by the production of mineral phases. BBA experiences extensive chemical aging as the smoke plume dilutes and we explored how this alters the ice activity of the smoke using simulated atmospheric aging of authentic BBA in a chamber reactor. Surprisingly, atmospheric aging enhanced the ice activity for most types of fuels and aging schemes. The removal of organic carbon particle coatings that conceal the mineral-based ice-active sites by evaporation or oxidation then dissolution can increase the ice activity by greater than an order of magnitude. This represents a new framework for the evolution of INPs from biomass burning where BBA becomes more ice active as it dilutes and ages, making a larger contribution to the INP budget, resulting cloud microphysics, and climate forcing than is currently considered.

Introduction

Biomass burning occurs globally year-round, releasing complex mixtures of organic and inorganic gaseous and particulate components, minerals, ash, and elemental carbon (soot) to the atmosphere, often in major episodic wildfire events that greatly perturb the Earth-cloud-climate system (1). This burning of plant material occurs naturally in forest fires or can be initiated by prescribed burns or by accidental human activity. With the growth of drought-stricken regions, wildfires are expected to increase in extent and severity and occur in regions not historically prone such as the southeastern United States (2–5). Biomass-burning aerosol (BBA) represents a large fraction of global particulate matter, contributing three-quarters of the total carbonaceous aerosol burden and over one-third of total black carbon emissions (6, 7). BBA composition is complex, including organic carbon, elemental carbon, tarballs, minerals, ash, and inorganic salt phases, and this composition determines the aerosol properties and their effects on the atmosphere and climate systems (8–13).

BBA can directly influence the Earth's radiative balance through the light absorbing properties of the black and brown carbon present, and the light scattering effects of the aerosol. Indirectly, BBA can affect cloud formation and precipitation through its ability to act as cloud condensation nuclei (CCN) (14–16) or ice nucleating particles (INPs). Cloud glaciation – which requires INPs to catalyze heterogeneous ice nucleation at temperatures warmer than –35 °C – affects the structure, lifetime, precipitation, and radiative properties of clouds. Accurate modeling of the Earth–climate system therefore requires achieving a much more complete understanding of heterogeneous ice nucleation and the sources and properties of different types of INPs (17–19). Considering the sheer mass of BBA emitted globally and the potential impacts of INPs on many atmospheric processes, the intersection of these two topics requires greater attention.

The fraction of BBA particles that are INP and their ice-nucleating abilities and freezing temperatures greatly vary depending on the type of fuel and combustion conditions (20-25). The first direct evidence of INPs released during biomass-burning events was only reported about ten years ago, wherein INPs were detected in the smoke of 9 out of 21 biomass fuels tested in laboratory studies (22). The authors estimated that BBA is an important source of ice nucleating particles that leads to atmospheric INP concentrations that can significantly alter cloud properties on a regional scale. Further experiments detected INPs in the smoke of 13 out of 22 fuels tested, with the highest concentrations found during intense flaming combustion (23). Prenni et al. sampled ambient air downwind of prescribed burns and wildfires and detected high number concentrations of INPs during flaming-phase combustion (25). In other field measurements INP concentrations were elevated during biomass-burning events, but the authors noted that soil lofted due to the intense fires may have contributed to the measured INPs (20). Most recently in Jahn et al. we demonstrated that new crystalline mineral phases produced during biomass combustion (i.e. not from lofted soil) are present in both the aerosol and remaining bottom ash. We concluded these minerals are the major source of ice nucleants in BBA, inducing immersion freezing at temperatures up to -13 °C, well above the temperatures at which graphitic soot particles can nucleate ice (26). This suggests that the common assumption that the lofting of already existing dust and soil particles or the presence of ice-active carbonaceous soot particles are the major sources of INPs often found in BBA is inaccurate or incomplete.

54

55

56

57

58

59 60

61

62 63

64 65

66

67

68 69

70

71

72 73

74 75

76 77

78 79

80

81

82

83

84 85

86

87 88

89

90 91

The vast majority of studies of INPs from biomass burning have only examined freshly emitted aerosol particles or smoke intercepted of unknown atmospheric age. Yet, studies on the atmospheric processing of mineral-based INPs have revealed significant changes in icenucleation activity (INA) in some cases (27–30), suggesting that atmospheric processing may change the mineral-based INPs emitted in BBA. Although we recently established that carbonaceous soot cannot explain the ice nucleation we observe in a variety of nascent BBA from different fuels, it has been established that oxidative aging of graphitic soot surfaces can promote ice-nucleation activity (31). These previous aging studies on single-component systems likely do not apply to BBA because of its complex heterogeneous composition, and only a few studies have examined authentic aged BBA. The photochemical aging of wood BBA in a chamber reactor was shown to have no effect on its INA, although the INA of this particular unaged BBA was quite low to begin with, only inducing immersion freezing at -35 °C (24). Conversely, wildfire smoke aerosol that travelled 1600 km had the highest ice-active particle number fraction out of all fires in one field study, suggesting that atmospherically aged BBA does retain its ice-nucleating ability or perhaps even experiences an enhancement in INA (25). Taken together these findings suggest that there are strong yet unconstrained possibilities for alteration of the ice-nucleating ability of the mostly mineral-based INPs in BBA through atmospheric aging processes.

We have essentially no understanding of the susceptibility of these largely mineral-based biomass-burning INPs to atmospheric chemical aging processes or to what extent aging might alter these critical properties required for modeling the interactions of BBA with cloud systems and the hydrological cycle. Aerosol particles have atmospheric lifetimes of a week or more and the composition and properties of BBA change rapidly as the smoke plume dilutes and mixes with external reactants and oxidants. We therefore sought to investigate how the immersion freezing ice-nucleating ability of BBA is altered during atmospheric transport such as through evaporation and (photo)oxidation mechanisms by performing controlled simulated aging of BBA produced from the combustion of authentic fuels. We found that evaporation through dilution and exposure to oxidants often results in an increase in the INA of BBA, suggesting that biomass-burning plumes likely have more extensive effects on cloud microphysical properties and climate over larger spatial extents as the smoke is transported through the atmosphere than previously recognized.

Results

92

93

94

95

96

97

98

99

100 101

102

103

104

105

106

107

108

109

110

111

112

113114

115

116

117

118

119

120 121

122

123

124

125

126127

128

129

Authentic biomass fuels collected within the United States were burned, and the emissions from this open combustion were injected into a large Teflon smog chamber reactor (see Figure S1 for an experimental schematic). The fuels selected are representative of those commonly burned in the western and southeastern United States during wildfires and prescribed burns. The size distribution and chemical composition of the resulting aerosol particles were analyzed online, and particles were also collected on various substrates for subsequent offline analysis. After the completion of each burn and chamber filling, a 10-minute waiting period allowed for initial mixing of the aerosol in the chamber. Then, a "fresh" aerosol filter sample was collected from the chamber for two hours. Four types of aging were conducted: 1) no external perturbation or oxidants added ('time aging'); 2) hydroxyl radical (·OH) oxidation with added nitrogen oxides (NO_x); 3) removal of organic aerosol (OA) and other semi-volatile components using a thermodenuder prior to injection into the chamber, followed by ·OH oxidation; 4) injection of ozone with no UV photolysis (dark ozonolysis). After the simulated aging was completed, another mixing period of 10-20 minutes took place, and a separate "aged" filter sample was collected for the last two hours of the experiment. The BBA was extracted by vortexing each filter in filtered water to assess the immersion freezing ice-nucleation activity (INA) using a novel microfluidic device (see Methods section for additional details) (32). The INA of fresh BBA between different experiments varies due to natural burn-to-burn variability that results from different combustion conditions at the microscale; previous experiments on the ice nucleating ability of BBA have also observed this natural variability (22, 23). The discussion of changes in INA with simulated atmospheric aging below always compares the fresh and aged aerosol within the same chamber experiment to account for this variability.

Enhancement of ice activity following time aging and evaporation of organic aerosol

The immersion-mode INA of the 'time aged' BBA collected between four to six hours after it remained in the chamber following injection and dilution of the emissions was notably increased for sawgrass and cutgrass BBA compared to BBA collected during the first two hours of each experiment (Figure 1a). These time aging experiments were conducted with no external oxidants added or other perturbations to compare to the stronger forced perturbations used in subsequent experiments; the BBA experiences appreciable evaporation just by dilution of the nascent smoke into the chamber. This increase in INA induced by several hours of holding the aerosol in the Teflon chamber is surprising given that any oxidants present in the nascent BBA would be quickly depleted – the elemental O:C (a measure of the OA oxidation state) for time aging experiments increased on the order of 30%, while other more aggressive aging regimes increased the OA oxidation state by > 90%. The increase in INA (*n*₅) here is larger than observed when external perturbation and/or oxidants were applied, as presented below.

Aerosol composition measurements indicate substantial evaporative loss of organic aerosol, seen through the decrease in the organic aerosol-to-black carbon (a conserved tracer) mass ratio (OA:BC) by up to 20% (Fig. 2a). BBA is well known to contain OA of intermediate to low volatility (their saturation vapor pressure) that can experience significant evaporation through smoke plume dilution (33, 34), and vapor wall losses in Teflon chambers promote evaporation in laboratory experiments. The organic aerosol is heterogeneously distributed throughout the complex BBA and is often non-uniformly mixed in individual submicron particles that also contain soot, inorganic salts, and/or mineral phases (26). The evaporation of semi-volatile OA observed here would reveal more of the ice-active surface sites already present in the BBA, allowing them to interact directly with water and nucleate ice that cannot occur when the sites are concealed. This explains the large increase in ice activity observed in the aged BBA and the sharp increase in the ice-active site density (n_s) over a narrow temperature range, which indicates the ice nucleants in both fresh and aged BBA have similar properties. BBA produced by the combustion of ponderosa pine needles contains many fewer Si-containing mineral particles compared to the grass fuels, which could explain why an increase in INA was not observed for this fuel type (26).

Enhancement of ice activity through photooxidative aging

Consistent increases in INA following hydroxyl radical (\cdot OH) aging under high NO_x conditions were demonstrated across most temperatures for all fuel types (Figure 1b), although the changes were smaller than in our time aging experiments with no added oxidants. Similar to the time aging experiments, the ponderosa pine needle BBA had the smallest increase in INA, only increasing at temperatures below –29.5 °C. The hydroxyl radical is an important and powerful atmospheric oxidant and was generated by UV photolysis of nitrous acid (HONO) injected into the chamber. The increase in INA could be due to oxidation of graphitic soot particle surfaces, oxidation of mineral surfaces, or possibly

due to changes in the organic aerosol components that are prone to ·OH oxidation. BBA that is dominated by black carbon and does not contain many mineral species as identified by TEM/EDX particle analysis tends to have low INA that does not increase with photooxidation. This is presumably because there are limited mineral-based ice-active sites to uncover; see Fig. S4 in the Supplementary Materials for further explanation.

In order to understand how changes to the OA components could explain the observed increases in INA, we compared the volatility of fresh and aged biomass-burning OA by measuring the mass fraction remaining following thermal desorption at different temperatures up to 200 °C (Fig. S5) (35). The aged aerosol consistently lost less OA mass than the fresh aerosol at every desorption temperature, indicating that aged BBA is less volatile than the fresh aerosol, similar to previous findings (36, 37). This supports what was also observed in time-aging experiments where the more volatile OA present at the beginning of the experiments evaporated, uncovering ice-active surface sites and increasing the INA of aged BBA samples. Thermodenuder analysis also showed that the carbon oxidation state of the remaining organic aerosol components increased as indicated by an increased oxygen-to-carbon mass ratio following aging, corresponding to their decreased volatility (Fig. 2b). Since oxidation can also increase volatility through the organic carbon backbone fragmentation channel, the less-volatile OA observed here is the result of components that gained more oxygenated functional groups while avoiding fragmentation (38).

Oxidation of organic carbon molecules tends to increase hydrophilicity and water solubility, such that the removal of OA from ice-active sites may be promoted by dissolution following oxidative aging. This mechanism would be highly relevant for immersion-mode freezing in mixed-phased clouds – the dominant heterogeneous ice nucleation mechanism that we studied here where the INP is immersed in a cloud droplet prior to nucleating ice. Liquid droplets containing these INPs may exist long enough prior to experiencing freezing conditions such that the more viscous, low-volatility organic compounds also dissolve and reveal ice-active sites in addition to the prompt removal of the more water-soluble oxidized organic carbon.

Alteration of ice activity from photooxidation following thermal evaporation of semi-volatile aerosol components

No consistent trend in INA was observed following the photooxidation of BBA that had first been subjected to thermal desorption (Figure 1c). In these experiments, most OA was removed by passing the biomass emissions through a thermodenuder heated to 250 °C prior to injection into the smog chamber. A smaller amount of organic mass entered the chamber compared to unheated BBA; refer to Figure 2c for an example of aerosol composition. This method allowed us to examine the INA of the initial aerosol population stripped of most of the OA. The subsequent addition of the hydroxyl radical directly targets the oxidative aging

of the aerosol composed of the remaining very low volatility organic carbon components, inorganics, minerals, and graphitic soot.

205

206

207

208

209210

211

212

213

214

215

216217

218

219220

221

222223

224

225226

227

228229

230

231232

233

234

235

236

237

238239

240

241242

In the cutgrass experiment there was a sharp increase in the ice-active site density specifically at -23 °C following thermal evaporation then oxidation. This suggests an enhancement in a specific type of ice-active site because of the large increase in INA in a narrow temperature range. One possible type is the mineral phases present in BBA, which could more effectively nucleate ice upon exposure to the hydroxyl radical, especially since the removal of the more volatile OA in the thermodenuder would expose more of the mineral surfaces. Another candidate ice-active site in BBA is graphitic soot, whose surfaces could also become exposed after the removal of the more volatile OA. ·OH oxidation could also produce surface hydroxyl groups on the graphitic surfaces that will interact strongly with water through hydrogen bonding. The molecular dynamics simulations of Lupi and Molinero revealed that OH-modified graphitic surfaces were more effective at inducing freezing than unmodified graphitic surfaces (39). Increased hydrophilicity of soot particles through atmospheric aging has been demonstrated experimentally to increase INA at cirrus cloud temperatures < -40 °C (31, 40-42). While authentic combustion soot particles are not typically ice active at mixed-phase cloud temperatures > -35 °C (31, 43-45), it is possible that the soot particles emitted from some types of biomass fuel combustion are ice active at warmer temperatures than soot from fossil fuel combustion, and/or that these BBA soot particle surfaces are more susceptible to enhancements in INA through oxidation.

In the sawgrass experiment, the denuded fresh and aged aerosol had nearly the same INA. The BBA from the cutgrass and sawgrass experiments shown in Fig. 1c had similar black carbon content (48% and 53%, respectively) following evaporation in the thermodenuder before entering the chamber, and so the observed differences in INA are not simply due to black carbon. While the trends in INA for the thermally denuded aerosol vary by experiment, it is noteworthy that these experiments with most OA removed still result in ice-active site densities above background levels and within the same orders of magnitude as unaltered fresh BBA. This further supports the idea that ice-active sites in BBA active under immersion-freezing conditions are not organic carbon-based. Our prior analysis of the BBA and ash produced from these same fuels concluded that the production of new mineral phases from the biomass combustion itself is the major source of the ice nucleants, and that fuels that produced the most soot had the weakest or even unmeasurable INA at temperatures warmer than –25 °C (26). These observations are supported by a recent study of prescribed burns and wildfires that estimated that black carbon contributed at most 10% to observed INP concentrations (44).

Impairment of ice activity from production of secondary organic aerosol by dark ozonolysis

The INA of BBA subjected to dark ozonolysis was lower than that of fresh aerosol in some cases, likely due to the production of secondary organic aerosol that covered ice-active

surface sites (Fig. 1d). In this aging mechanism ~300 ppb of ozone was injected into the chamber with no UV light illumination. Previous studies have shown that dark ozonolysis reliably produces significant SOA mass and the largest increase in total OA from biomass-burning emissions, making this aging mechanism a good test for the effects of SOA production and OA particle coatings on ice activity (46, 47). Note that some ·OH is still generated without UV photolysis, produced by the ozonolysis of unsaturated organic molecules such as monoterpenes or alkenes (46, 48). Dark ozonolysis did result in the greatest SOA production compared to other aging mechanisms, with the OA:BC mass ratio increasing by up to 25%, as shown in Figure 2d.

The fresh and aged BBA had essentially the same ice-nucleating abilities following dark ozonolysis or even a decrease in INA for the cutgrass experiment (Fig. 1d). We attribute this to increasing SOA coating amount and thickness on the BBA, counteracting the effects of the evaporation and oxidation plus dissolution of OA observed in the time aging and ·OH aging experiments. These results also indicate that the SOA coatings are not sufficiently removed when the aerosol is extracted into water for immersion freezing analysis, perhaps because the SOA generated during dark ozonolysis is less fragmented and of lower water solubility and therefore remains concealing the ice-active sites. The already existing primary hydrocarbon-like OA likely only partially coats the highly heterogeneous BBA particles and SOA production may also act to more completely coat the complex aerosol through condensation of oxidized OA. Indeed SOA of an oxidation state similar to the O:C of the aged BBA in our experiments is often found to phase separate from the aqueous phase and adopt a core–shell morphology with the organic phase on the outside (49).

Analysis of individual biomass-burning aerosol particles

The collected BBA was analyzed at a single-particle level using transmission electron microscopy (TEM) to investigate the potential particle types that are responsible for the observed ice activity and how these respond to the simulated aging. Many mineral-based particles coated in organic carbon phases were observed. Figure 3a shows a fractal soot particle that is agglomerated with an iron-based mineral as determined by energy dispersive X-ray (EDX) spectroscopy. The particle in Figure 3b contains potassium chloride salts and a mineral core made of magnesium, aluminum, silicon, and oxygen, also surrounded by an organic coating that appears to have partially evaporated under the vacuum of the TEM. The particle in Figure 3c has several inorganic salt phases surrounded by a dense organic carbon coating. These particle types and mixtures are all representative of fresh BBA filter samples where heterogeneous ice nucleation was observed above –25 °C. Note that the small < 500 nm size of the mineral components suggests that these were formed during combustion, as the majority of minerals lofted by mechanical action from soil dust or biomass ash would be supermicron. In our previous work, the most crystalline mineral phases were present in all samples of both aerosol and ash from the tall grass fuels, which also contain more INPs and

have higher INA than BBA from wood fuels (26). As most mineral particles in the BBA were found to be submicron, these potential INPs will have longer lifetimes versus gravitational settling, undergo atmospheric transport over longer distances, and exert more extensive effects on cloud microphysics over larger spatial scales than the much larger supermicron lofted ash particles would (26).

Discussion

Simulated atmospheric aging indicates that the ice-nucleation activity and INP number concentration of authentic BBA would generally increase as the aerosol undergoes atmospheric transport, though plume dilution must also be accounted for. The evaporation of organic coatings off the BBA reveals mineral-based ice-active sites, increasing the ice-nucleating ability of the BBA during most experiments. Simulations based off of FLAME III biomass-burning experiments estimated that 35% of the loss of OA after combustion was due to organic evaporation driven by loss of semi-volatile OA following smoke dilution into the chamber and vapor partitioning to the chamber walls (50). Fresh BBA is composed of 20-90% organic carbon compounds, a substantial fraction of which are known to evaporate upon dilution from near-fire to dispersed plume aerosol concentrations, but overall evaporation rates and partitioning depends on many factors such as aerosol mass loading, fuel type and combustion conditions, and dilution rate (33). These factors also contribute to the variability in INA amongst other studies of INPs from biomass burning.

Loss of OA through natural evaporation was observed at the beginning of nearly all chamber experiments, and in the time aging and ·OH photooxidation experiments, the OA:BC ratio remained fairly constant throughout the rest of these experiments. Therefore, these two aging mechanisms both resulted in similar trends in INA. The additional chemical oxidation during ·OH photooxidation experiments likely increased the water solubility of OA particle coatings, allowing for easier dissolution during immersion-mode experiments and uncovering of ice-active surface sites. However, more secondary organic aerosol (SOA) mass was generated during the latter part of the ·OH aging experiments compared to the time aging experiments where total OA only decreased in time. This may account for the smaller increase in ice-active site density following ·OH photooxidation by not resulting in as extensive an uncovering of ice-active sites as in the time aging experiments with more significant evaporation of OA. Direct oxidation of mineral surfaces within the BBA may have also led to the increased INA observed in aged BBA produced from mineral-rich grass fuels, but this mechanism could not be directly tested.

Even greater SOA production such as from dark ozonolysis (that avoids OA fragmentation by photolysis) further conceals ice-active sites on the particles, resulting in no increase or even a decrease in INA with aging. Previous literature has shown that SOA coatings can decrease the INA of other INPs in some instances. For example, Arizona test dust and the mineral dust illite were coated with SOA created from the ozonolysis of α -pinene, and aerosol

mass fractions percentages of SOA as low as 17% were found to decrease the deposition-mode INA of these atmospheric mineral dust proxies (27). However, the immersion-mode INA of desert mineral dusts did not significantly change when coated in SOA produced from α -pinene ozonolysis (51). Here, SOA produced by the dark ozonolysis of authentic biomass-burning smoke appears to be concealing the ice-active sites in BBA, presumably because the biomass burning SOA is more effective at covering the ice-active sites compared to prior terpene SOA coating experiments. The SOA produced here may also be less volatile and more viscous than the proxy SOA created through α -pinene ozonolysis and therefore remain concealing ice-active sites during immersion-mode freezing. These explanations are just reasonable predictions based off of prior knowledge of how the deposition and immersion-mode freezing of mineral particle systems respond to surface coatings, but they are supported by our immersion freezing experiments and aerosol composition data (28, 29). While different studies demonstrate variable degrees of SOA production or OA loss in biomass-burning plumes, our results are relevant for plumes that undergo significant SOA production, such as those from larger fires in more polluted areas (52, 53).

Figure 4 illustrates a new framework to understand how INPs from biomass burning and their chemical composition and ice-nucleation activity co-evolve during plume dilution and atmospheric processing based on these new findings. Evaporation of organic aerosol occurs to different extents following the emission and dilution of the smoke and leads to an increased availability of ice-active surface sites. Photooxidation of organic compounds changes the chemical composition to produce more oxidized OA with increased water solubility such that when the particle is immersed in a cloud droplet prior to undergoing immersion freezing, the OA can dissolve more readily to reveal ice-active sites. Condensation of SOA, driven by more oxidized and less volatile OA produced from evaporated organic carbon (that avoids the fragmentation channel), conceals ice-active sites on the particles and decreases the apparent INA. Authentic biomass-burning plumes undergo varying degrees of evaporation, oxidation, and re-condensation of organic aerosol (47, 54, 55). These processes compete simultaneously to different degrees, depending on fuel composition, combustion conditions, dilution ratios, and atmospheric conditions surrounding biomass plumes that entrain background air and reactants into the plume as it dilutes and spreads (53). Therefore, all these processes must be taken into account when considering the INA of BBA during or following atmospheric aging.

This work is the first to investigate how INPs released by the combustion of several different biomass fuels evolve under different simulated atmospheric aging schemes. A strong enhancement of the INA through some types of atmospheric aging was discovered. INA increased more after aging in BBA produced by the combustion of grassy fuels – which have a much higher mineral content – than other fuels like pine needles and woods that produce BBA with higher organic aerosol and black carbon content instead. These differences can be attributed to the observed changes in particle properties and composition

that lead to an uncovering of pre-existing ice-active surface sites that we recently demonstrated are mostly mineral phases produced by the biomass combustion itself (13, 26). TEM images of the BBA collected in these experiments also clearly show mineral phases and their mixtures with other particle components such as BC soot and salt phases that are often coated by organic carbon.

Here, we show how the INA of biomass-burning aerosol can be enhanced through some types of relevant atmospheric aging mechanisms. Unlike many previous studies that have shown that the INA of mineral dust particles can sometimes be impaired through atmospheric aging, here we find some types of aging actually enhance the INA of BBA (27–29, 56). The different effects of aging for these two mineral-containing aerosol systems are due to the presence of primary components emitted in the nascent BBA that can conceal the ice-active particle surfaces such as the mineral phases. Aging can lead to the partial removal of these coatings, thus increasing the INA. Mineral dust particles do not typically contain primary particle coatings that resist dissolution such as the hydrocarbon-like tar material common in BBA (8, 11, 57). For atmospheric mineral dust, coatings are acquired through atmospheric aging thus concealing or chemically altering ice-active surface sites with soluble inorganic components or oxidized SOA that sometimes lead to a decrease in INA.

Dilution, evaporation, and exposure of the BBA to oxidants often results in an increase of ice-active site density greater than an order of magnitude even at temperatures above -25 °C and an increase in the onset freezing temperature of up to 8 °C. This process would likely be enhanced under many atmospherically relevant scenarios as OA evaporation is driven more rapidly and extensively by the continual dilution of the smoke plume during transport that proceeds for several days or even weeks for submicron aerosol; most of the mineral particles observed in the BBA that are the likely source of ice nucleation were submicron in size. Removal of these OA coatings can also make reactive mineral and halide salt phases available for direct reaction with atmospheric reactants, such as the activation of chlorine as ClNO₂(g) and HCl(g) from Cl⁻(aq) through reactive uptake of N₂O₅(g) that we have recently demonstrated in BBA (58, 59).

The implications of this new framework for the co-evolution of biomass-burning aerosol composition and ice-nucleation activity are that the emitted ice nucleating particles will make important contributions to the distribution of atmospheric INPs over larger spatial and temporal extents and at warmer cloud temperatures than previously understood. In fact, the effective concentration of INPs emitted in BBA will increase during plume dilution as particle coatings experience net evaporation, until dilution of the aerosol particle numbers overcomes this effect. Previous estimates of the INP concentration in fresh BBA emitted during wildfires include 10^6 – 10^{15} INPs per m² of burned land (active at –30 °C) based on a variety of tested fuels, and 5×10^{10} – 1×10^{12} INPs per m² of burned grassland (active at –25 °C) based on our recent report on INPs emitted by combustion of tall grasses. This estimate of

INP emissions results in an area of 10⁴ km² with a 5 km plume height having INP concentrations elevated above typical background levels due to biomass burning and likely sufficient to modify cloud microphysics, from just 1 m² of burned land (*22, 26*). Our results presented here show that atmospheric aging enhances the ice-active site density by up to a factor of 27 at –25 °C. Therefore, atmospheric aging of BBA could increase the area affected by INPs by at least one decade, causing an estimated area of 10⁵ km² by 5 km in altitude to be affected for each 1 m² of burned grassland. These observed increases in ice activity in terms of both INP concentration and freezing temperature are substantial considering the vast areas of biomass consumed in wildfires, especially in recent years. Fully understanding the impacts of this newly understood dynamic evolution of the INPs in BBA requires investigation using chemical transport models that properly account for the evolution of BBA composition during atmospheric transport (*33, 60*).

Methods

A small portion of each biomass fuel was placed into a partially enclosed galvanized steel pan and lit from the side with a butane lighter. The remaining biomass fuel was gradually added to maintain flaming phase combustion, until a total of 0.5 kg was burned. The fuels used were giant cutgrass (zizaniopsis miliacea), obtained at the UF/IFAS Center for Aquatic and Invasive Plants in Florida, USA; ponderosa pine needles (pinus ponderosa) obtained at the Klamath Basin National Wildlife Refuge Complex in Tulelake, California, USA; sawgrass (cladium jamaicense), obtained at the Loxahatchee National Wildlife Refuge in Florida, USA; and birch and fatwood logs, purchased locally. The smoke emissions were injected and diluted using Dekati eductor diluters (Dekati DI-1000) into a 12 m³ Teflon smog chamber (26, 59). Before each experiment, the chambers were purged overnight using filtered clean air and UV lights until particle number concentrations were < 50 cm⁻³. No artificial circulation mechanism was used in the chamber apart from some possible natural convection due to temperature gradients. The only times when the air within the chamber is turbulent is during aerosol injection and injection of HONO or ozone vapor; during these times we did not collect filters for ice-nucleation activity analysis. For the BBA present in these chamber experiments, given the small particle size (geometric mean diameter ~200 nm) and low concentration (< 10⁵ #/cm³), gravitational settling is not significant and there is also no significant associated coagulation under the experimental timescales (61). Particle wall loss was the dominant loss mechanism and is mainly driven by electrostatic forces close to the Teflon chamber walls and there are no differences in the prevailing particle loss mechanisms or rates between the fresh and aged time periods that would affect our results.

Online particle analysis included a scanning mobility particle sizer (SMPS, TSI Inc.: DMA model 3082 and CPC model 3775) for aerosol size distribution measurements between 8 and 749 nm in mobility diameter, and a soot-particle aerosol mass spectrometer (SP-AMS, Aerodyne Inc.) for submicron particle chemical characterization. The SP-AMS uses an

infrared laser to measure refractory black carbon (BC) soot, and the instrument was operated with switching the IR laser on/off every 60 seconds (*62*). During both modes, a 600 °C tungsten thermal vaporizer was used to vaporize non-refractory aerosol components: organic carbon aerosol (OA), nitrate, sulfate, chloride, and ammonium. Laser-on (BC) mode was used to obtain the mass concentrations shown in Figure 2, and the O:C mass ratio was determined from laser-off (EI) mode. For volatility analysis, the aerosol was alternated between passing through a heated thermodenuder (centerline residence time of 23 s) or through an unheated bypass line before being sampled by the SP-AMS. Gas monitors included a chemiluminescent NO_x analyzer (Advanced Pollution Instrumentation, Inc., Model 200A) and an ozone analyzer (Teledyne, Model T400). Particles were collected onto copper formvar TEM grids (carbon type B, 400 mesh, Ted Pella #01754-F) for offline electron microscopy analysis. TEM/EDX measurements were acquired at the Environmental Molecular Sciences Laboratory (EMSL) at PNNL using a Titan 80-300 scanning/transmission electron microscope equipped with an Si(Li) detector at an accelerating voltage of 300 keV.

Particles were collected for ice nucleation analysis on polycarbonate filters (GE Healthcare 111103, Nuclepore 50 nm pore size) using an inline 44 mm filter holder and refrigerated until use. Immediately before analysis, particles were extracted off of the filter by vortexing the filter in a polypropylene Falcon tube with 3 mL of HPLC-grade water (Sigma Aldrich HPLC Plus #34877) that was pre-filtered (Anotop 25 Plus 0.02 µm pore size, Whatman #6809-4102), as this results in the lowest level of background freezing (63). The suspension was then filled into a custom microfluidic chip where 600 uniformly sized isolated 6 nL droplets are produced and can be tested simultaneously with a background freezing temperature for filtered water of < -33 °C (32). The chip was placed atop a thermoelectric cooling element and cooled at 1 °C min⁻¹, with droplet freezing detected using the observed change in grayscale value. For some earlier experiments presented in the Supplementary Materials, the droplet freezing assay was performed using a conventional droplet-on-substrate method and 0.1 µL droplets (63). Filtered water background freezing occurred well-below the droplet freezing temperature observed of the BBA samples, and the frozen fraction spectra of handling filter blanks were slightly higher than filtered water background freezing but still much lower than most BBA samples; see Figure S7 for additional information. The ice-active surface site density (n_s) was calculated using the total surface area of the collected aerosol samples based off of the total air volume passed through the filters and an averaged aerosol size distribution measured by SMPS throughout the fresh or aged BBA collection period (64). To ensure that the observed trends in INA with aging were not simply due to artifacts in how the aerosol surface area distribution (used to calculate n_s) changes with time across each experiment, we normalized the ice-nucleation activity to the aerosol mass concentration of black carbon, as shown in Fig. S9. This method of normalizing the INA to a conserved nonvolatile aerosol tracer reveals the same trends in INA for all four aging mechanisms as are shown in Fig. 1. Changes in the aerosol size distribution and surface area therefore do not explain the observed changes in the INA following various types of simulated atmospheric aging.

475

476

References

- 1. M. Fromm, D. Peterson, L. Di Girolamo, The primary convective pathway for observed wildfire emissions in the upper troposphere and lower stratosphere: a targeted reinterpretation. *J. Geophys. Res. Atmos.*, 2019JD031006 (2019).
- C. S. Stevens-Rumann, K. B. Kemp, P. E. Higuera, B. J. Harvey, M. T. Rother, D. C.
 Donato, P. Morgan, T. T. Veblen, F. Lloret, Ed., Evidence for declining forest resilience to wildfires under climate change. *Ecol. Lett.* 21 (2018), pp. 243–252.
- 483 3. K. O'Dell, B. Ford, E. V Fischer, J. R. Pierce, Contribution of Wildland-Fire Smoke to US
 484 PM 2.5 and Its Influence on Recent Trends. *Environ. Sci. Technol.* **53**, 1797–1804
 485 (2019).
- 486 4. C. D. McClure, D. A. Jaffe, US particulate matter air quality improves except in wildfire-prone areas. *Proc. Natl. Acad. Sci. U. S. A.* **115**, 7901–7906 (2018).
- 488 5. A. P. Williams, J. T. Abatzoglou, A. Gershunov, J. Guzman-Morales, D. A. Bishop, J. K. Balch, D. P. Lettenmaier, Observed Impacts of Anthropogenic Climate Change on Wildfire in California. *Earth's Futur.* **7**, 892–910 (2019).
- T. C. Bond, S. J. Doherty, D. W. Fahey, P. M. Forster, T. Berntsen, B. J. DeAngelo, M. G.
 Flanner, S. Ghan, B. Kärcher, D. Koch, S. Kinne, Y. Kondo, P. K. Quinn, M. C. Sarofim,
 M. G. Schultz, M. Schulz, C. Venkataraman, H. Zhang, S. Zhang, N. Bellouin, S. K.
 Guttikunda, P. K. Hopke, M. Z. Jacobson, J. W. Kaiser, Z. Klimont, U. Lohmann, J. P.
 Schwarz, D. Shindell, T. Storelvmo, S. G. Warren, C. S. Zender, Bounding the role of
 black carbon in the climate system: A scientific assessment. *J. Geophys. Res. Atmos.* 118, 5380–5552 (2013).
- 498 7. M. S. Reddy, O. Boucher, A study of the global cycle of carbonaceous aerosols in the LMDZT general circulation model. *J. Geophys. Res.* **109**, D14202 (2004).
- K. Adachi, A. J. Sedlacek, L. Kleinman, S. R. Springston, J. Wang, D. Chand, J. M. Hubbe,
 J. E. Shilling, T. B. Onasch, T. Kinase, K. Sakata, Y. Takahashi, P. R. Buseck, Spherical
 tarball particles form through rapid chemical and physical changes of organic matter
 in biomass-burning smoke. *Proc. Natl. Acad. Sci. U. S. A.* 116, 19336–19341 (2019).
- 9. P. J. Silva, D.-Y. Liu, C. A. Noble, K. A. Prather, Size and Chemical Characterization of Individual Particles Resulting from Biomass Burning of Local Southern California Species. *Environ. Sci. Technol.* **33**, 3068–3076 (1999).
- J. Li, M. Pósfai, P. V. Hobbs, P. R. Buseck, *J. Geophys. Res. Atmos.*, in press,
 doi:10.1029/2002JD002310.

- A. J. Sedlacek, P. R. Buseck, K. Adachi, T. B. Onasch, S. R. Springston, L. Kleinman,
 Formation and evolution of tar balls from northwestern US wildfires. *Atmos. Chem. Phys.* 18, 11289–11301 (2018).
- J. S. Reid, R. Koppmann, T. F. Eck, D. P. Eleuterio, A review of biomass burning
 emissions part II: Intensive physical properties of biomass burning particles. *Atmos. Chem. Phys.* 5 (2005), pp. 799–825.
- 515 13. S. V. Vassilev, D. Baxter, C. G. Vassileva, An overview of the behaviour of biomass 516 during combustion: Part I. Phase-mineral transformations of organic and inorganic 517 matter. *Fuel.* **112** (2013), pp. 391–449.
- M. D. Petters, C. M. Carrico, S. M. Kreidenweis, A. J. Prenni, P. J. DeMott, J. L. Collett, H.
 Moosmüller, Cloud condensation nucleation activity of biomass burning aerosol. *J. Geophys. Res.* 114, D22205 (2009).
- T. L. Lathem, A. J. Beyersdorf, K. L. Thornhill, E. L. Winstead, M. J. Cubison, A.
 Hecobian, J. L. Jimenez, R. J. Weber, B. E. Anderson, A. Nenes, Analysis of CCN activity
 of Arctic aerosol and Canadian biomass burning during summer 2008. *Atmos. Chem. Phys.* 13, 2735–2756 (2013).
- 525 16. G. J. Engelhart, C. J. Hennigan, M. A. Miracolo, A. L. Robinson, S. N. Pandis, Cloud 526 condensation nuclei activity of fresh primary and aged biomass burning aerosol. 527 *Atmos. Chem. Phys.* **12**, 7285–7293 (2012).
- 528 17. P. J. DeMott, A. J. Prenni, X. Liu, S. M. Kreidenweis, M. D. Petters, C. H. Twohy, M. S. Richardson, T. Eidhammer, D. C. Rogers, Predicting global atmospheric ice nuclei distributions and their impacts on climate. *Proc. Natl. Acad. Sci.* **107**, 11217–11222 (2010).
- J. H. Seinfeld, C. Bretherton, K. S. Carslaw, H. Coe, P. J. DeMott, E. J. Dunlea, G.
 Feingold, S. Ghan, A. B. Guenther, R. Kahn, I. Kraucunas, S. M. Kreidenweis, M. J.
 Molina, A. Nenes, J. E. Penner, K. A. Prather, V. Ramanathan, V. Ramaswamy, P. J.
 Rasch, A. R. Ravishankara, D. Rosenfeld, G. Stephens, R. Wood, Improving our
 fundamental understanding of the role of aerosol-cloud interactions in the climate
 system. *Proc. Natl. Acad. Sci. U. S. A.* 113, 5781–5790 (2016).
- J. Fan, Y. Wang, D. Rosenfeld, X. Liu, Review of aerosol-cloud interactions:
 Mechanisms, significance, and challenges. J. Atmos. Sci. 73 (2016), pp. 4221–4252.
- C. S. McCluskey, P. J. DeMott, A. J. Prenni, E. J. T. Levin, G. R. McMeeking, A. P. Sullivan,
 T. C. J. Hill, S. Nakao, C. M. Carrico, S. M. Kreidenweis, Characteristics of atmospheric
 ice nucleating particles associated with biomass burning in the US: Prescribed burns
 and wildfires. J. Geophys. Res. Atmos. 119, 10458–10470 (2014).
- 544 21. P. J. DeMott, M. D. Petters, A. J. Prenni, C. M. Carrico, S. M. Kreidenweis, J. L. Collett, H. Moosmüller, Ice nucleation behavior of biomass combustion particles at cirrus

- temperatures. J. Geophys. Res. Atmos. 114, D16205 (2009).
- M. D. Petters, M. T. Parsons, A. J. Prenni, P. J. DeMott, S. M. Kreidenweis, C. M. Carrico,
 A. P. Sullivan, G. R. McMeeking, E. J. T. Levin, C. E. Wold, J. L. Collett, H. Moosmüller,
 Ice nuclei emissions from biomass burning. J. Geophys. Res. 114, D07209 (2009).
- 550 23. E. J. T. Levin, G. R. McMeeking, P. J. DeMott, C. S. McCluskey, C. M. Carrico, S. Nakao, T. Jayarathne, E. A. Stone, C. E. Stockwell, R. J. Yokelson, S. M. Kreidenweis, Icenucleating particle emissions from biomass combustion and the potential importance of soot aerosol. *J. Geophys. Res. Atmos.* **121**, 5888–5903 (2016).
- 554 24. C. Chou, Z. A. Kanji, O. Stetzer, T. Tritscher, R. Chirico, M. F. Heringa, E. Weingartner, 555 A. S. H. Prévôt, U. Baltensperger, U. Lohmann, Effect of photochemical ageing on the 556 ice nucleation properties of diesel and wood burning particles. *Atmos. Chem. Phys.* **13**, 557 761–772 (2013).
- 25. A. J. Prenni, P. J. Demott, A. P. Sullivan, R. C. Sullivan, S. M. Kreidenweis, D. C. Rogers,
 Geophys. Res. Lett., in press, doi:10.1029/2012GL051915.
- L. G. Jahn, M. J. Polen, L. G. Jahl, T. A. Brubaker, J. Somers, R. C. Sullivan, Biomass combustion produces ice-active minerals in biomass-burning aerosol and bottom ash. *Proc. Natl. Acad. Sci.* 117, 21928–21937 (2020).
- 563 27. O. Möhler, S. Benz, H. Saathoff, M. Schnaiter, R. Wagner, J. Schneider, S. Walter, V. Ebert, S. Wagner, The effect of organic coating on the heterogeneous ice nucleation efficiency of mineral dust aerosols. *Environ. Res. Lett.* **3** (2008), doi:10.1088/1748-9326/3/2/025007.
- R. C. Sullivan, M. D. Petters, P. J. Demott, S. M. Kreidenweis, H. Wex, D. Niedermeier,
 S. Hartmann, T. Clauss, F. Stratmann, P. Reitz, J. Schneider, B. Sierau, Irreversible loss of ice nucleation active sites in mineral dust particles caused by sulphuric acid condensation. *Atmos. Chem. Phys.* 10, 11471–11487 (2010).
- 571 29. R. C. Sullivan, L. Miñambres, P. J. Demott, A. J. Prenni, C. M. Carrico, E. J. T. Levin, S. M. Kreidenweis, Chemical processing does not always impair heterogeneous ice nucleation of mineral dust particles. *Geophys. Res. Lett.* **37**, 1–5 (2010).
- 574 30. G. R. Kulkarni, C. Sanders, K. Zhang, X. Liu, C. Zhao, Ice nucleation of bare and sulfuric 575 acid-coated mineral dust particles and implication for cloud properties. *J. Geophys.* 576 *Res. Atmos.* **119**, 9993–10011 (2014).
- 577 31. F. Mahrt, C. Marcolli, R. O. David, P. Grönquist, E. J. B. Meier, U. Lohmann, Z. A. Kanji, 578 Ice nucleation abilities of soot particles determined with the Horizontal Ice 579 Nucleation Chamber. *Atmos. Chem. Phys.* **18**, 13363–13392 (2018).
- T. Brubaker, M. Polen, P. Cheng, V. Ekambaram, J. Somers, S. L. Anna, R. C. Sullivan,
 Development and characterization of a "store and create" microfluidic device to
 determine the heterogeneous freezing properties of ice nucleating particles. *Aerosol*

- 583 *Sci. Technol.* **54**, 79–93 (2020).
- A. L. Hodshire, A. Akherati, M. J. Alvarado, B. Brown-Steiner, S. H. Jathar, J. L. Jimenez,
 S. M. Kreidenweis, C. R. Lonsdale, T. B. Onasch, A. M. Ortega, J. R. Pierce, Aging Effects
 on Biomass Burning Aerosol Mass and Composition: A Critical Review of Field and
 Laboratory Studies. *Environ. Sci. Technol.* 53 (2019), pp. 10007–10022.
- A. L. Robinson, N. M. Donahue, M. K. Shrivastava, E. A. Weitkamp, A. M. Sage, A. P.
 Grieshop, T. E. Lane, J. R. Pierce, S. N. Pandis, Rethinking organic aerosols:
 Semivolatile emissions and photochemical aging. *Science (80-.).* 315, 1259–1262
 (2007).
- 592 35. K. P. Cain, S. N. Pandis, A technique for the measurement of organic aerosol 593 hygroscopicity, oxidation level, and volatility distributions. *Atmos. Meas. Tech.* **10**, 594 4865–4876 (2017).
- C. Y. Lim, D. H. Hagan, M. M. Coggon, A. R. Koss, K. Sekimoto, J. De Gouw, C. Warneke,
 C. D. Cappa, J. H. Kroll, Secondary organic aerosol formation from the laboratory
 oxidation of biomass burning emissions. *Atmos. Chem. Phys.* 19, 12797–12809 (2019).
- 598 37. C. J. Hennigan, M. A. Miracolo, G. J. Engelhart, A. A. May, A. A. Presto, T. Lee, A. P.
 599 Sullivan, G. R. McMeeking, H. Coe, C. E. Wold, W.-M. Hao, J. B. Gilman, W. C. Kuster, J.
 600 A. De Gouw, B. A. Schichtel, J. L. Collett, S. M. Kreidenweis, A. L. Robinson, Chemical
 601 and physical transformations of organic aerosol from the photo-oxidation of open
 602 biomass burning emissions in an environmental chamber. *Atmos. Chem. Phys. Atmos.*603 *Chem. Phys.* **11**, 7669–7686 (2011).
- J. H. Kroll, N. M. Donahue, J. L. Jimenez, S. H. Kessler, M. R. Canagaratna, K. R. Wilson,
 K. E. Altieri, L. R. Mazzoleni, A. S. Wozniak, H. Bluhm, E. R. Mysak, J. D. Smith, C. E.
 Kolb, D. R. Worsnop, Carbon oxidation state as a metric for describing the chemistry
 of atmospheric organic aerosol. *Nat. Chem.* 3, 133–139 (2011).
- 608 39. L. Lupi, V. Molinero, Does hydrophilicity of carbon particles improve their ice 609 nucleation ability? *J. Phys. Chem. A.* **118**, 7330–7337 (2014).
- 40. K. A. Koehler, P. J. DeMott, S. M. Kreidenweis, O. B. Popovicheva, M. D. Petters, C. M.
 611 Carrico, E. D. Kireeva, T. D. Khokhlova, N. K. Shonija, Cloud condensation nuclei and
 612 ice nucleation activity of hydrophobic and hydrophilic soot particles. *Phys. Chem.* 613 *Chem. Phys.* 11, 7906 (2009).
- F. Mahrt, K. Kilchhofer, C. Marcolli, P. Grönquist, R. O. David, M. Rösch, U. Lohmann,
 Z. A. Kanji, The Impact of Cloud Processing on the Ice Nucleation Abilities of Soot
 Particles at Cirrus Temperatures. J. Geophys. Res. Atmos. 125 (2020),
 doi:10.1029/2019JD030922.
- F. Mahrt, P. A. Alpert, J. Dou, P. Grönquist, P. C. Arroyo, M. Ammann, U. Lohmann, Z.
 A. Kanji, Aging induced changes in ice nucleation activity of combustion aerosol as

- determined by near edge X-ray absorption fine structure (NEXAFS) spectroscopy. *Environ. Sci. Process. Impacts.* **22**, 895–907 (2020).
- 43. Z. A. Kanji, L. A. Ladino, H. Wex, Y. Boose, M. Burkert-Kohn, D. J. Cziczo, M. Krämer, *Meteorol. Monogr.*, in press, doi:10.1175/amsmonographs-d-16-0006.1.
- G. P. Schill, P. J. DeMott, E. W. Emerson, A. M. C. Rauker, J. K. Kodros, K. J. Suski, T. C. J.
 Hill, E. J. T. Levin, J. R. Pierce, D. K. Farmer, S. M. Kreidenweis, The contribution of
 black carbon to global ice nucleating particle concentrations relevant to mixed-phase
 clouds. *Proc. Natl. Acad. Sci. U. S. A.* 117, 22705–22711 (2020).
- 45. Z. A. Kanji, A. Welti, J. C. Corbin, A. A. Mensah, Black Carbon Particles Do Not Matter for Immersion Mode Ice Nucleation. *Geophys. Res. Lett.* **47**, 1–9 (2020).
- 46. D. S. Tkacik, E. S. Robinson, A. T. Ahern, R. Saleh, C. Stockwell, P. Veres, I. J. Simpson,
 S. Meinardi, D. R. Blake, R. J. Yokelson, A. A. Presto, R. C. Sullivan, N. M. Donahue, A. L.
 Robinson, A dual-chamber method for quantifying the effects of atmospheric
 perturbations on secondary organic aerosol formation from biomass burning
 emissions. J. Geophys. Res. Atmos. 122, 6043–6058 (2017).
- A. T. Ahern, E. S. Robinson, D. S. Tkacik, R. Saleh, L. E. Hatch, K. C. Barsanti, C. E.
 Stockwell, R. J. Yokelson, A. A. Presto, A. L. Robinson, R. C. Sullivan, N. M. Donahue,
 Production of Secondary Organic Aerosol During Aging of Biomass Burning Smoke
 From Fresh Fuels and Its Relationship to VOC Precursors. *J. Geophys. Res. Atmos.* 124,
 3583–3606 (2019).
- 48. S. E. Paulson, The reactions of ozone with alkenes: An important source of HOx in the boundary layer. *Geophys. Res. Lett.* **23**, 3727–3730 (1996).
- 49. K. Gorkowski, N. M. Donahue, R. C. Sullivan, Aerosol Optical Tweezers Constrain the
 643 Morphology Evolution of Liquid-Liquid Phase-Separated Atmospheric Particles.
 644 Chem. 6, 204–220 (2020).
- Q. Bian, A. A. May, S. M. Kreidenweis, J. R. Pierce, Investigation of particle and vapor wall-loss effects on controlled wood-smoke smog-chamber experiments. *Atmos. Chem. Phys.* 15, 11027–11045 (2015).
- Z. A. Kanji, R. C. Sullivan, M. Niemand, P. J. Demott, A. J. Prenni, C. Chou, H. Saathoff,
 O. Möhler, Heterogeneous ice nucleation properties of natural desert dust particles
 coated with a surrogate of secondary organic aerosol. *Atmos. Chem. Phys.* 19, 5091–
 5110 (2019).
- M. Shrivastava, C. D. Cappa, J. Fan, A. H. Goldstein, A. B. Guenther, J. L. Jimenez, C.
 Kuang, A. Laskin, S. T. Martin, N. L. Ng, T. Petaja, J. R. Pierce, P. J. Rasch, P. Roldin, J. H.
 Seinfeld, J. Shilling, J. N. Smith, J. A. Thornton, R. Volkamer, J. Wang, D. R. Worsnop, R.
 A. Zaveri, A. Zelenyuk, Q. Zhang, Recent advances in understanding secondary
- organic aerosol: Implications for global climate forcing. Rev. Geophys. **55**, 509–559

- 657 (2017).
- A. L. Hodshire, Q. Bian, E. Ramnarine, C. R. Lonsdale, M. J. Alvarado, S. M.
 Kreidenweis, S. H. Jathar, J. R. Pierce, More Than Emissions and Chemistry: Fire Size,
 Dilution, and Background Aerosol Also Greatly Influence Near-Field Biomass Burning
- 661 Aerosol Aging. J. Geophys. Res. Atmos. **124**, 5589–5611 (2019).
- L. A. Garofalo, M. A. Pothier, E. J. T. Levin, T. Campos, S. M. Kreidenweis, D. K. Farmer,
 Emission and Evolution of Submicron Organic Aerosol in Smoke from Wildfires in the
 Western United States. ACS Earth Sp. Chem. 3, 1237–1247 (2019).
- N. M. Donahue, S. A. Epstein, S. N. Pandis, A. L. Robinson, A two-dimensional volatility
 basis set: 1. organic-aerosol mixing thermodynamics. *Atmos. Chem. Phys.* 11, 3303–3318 (2011).
- D. J. Cziczo, K. D. Froyd, S. J. Gallavardin, O. Moehler, S. Benz, H. Saathoff, D. M.
 Murphy, Deactivation of ice nuclei due to atmospherically relevant surface coatings.
 Environ. Res. Lett. 4 (2009), doi:10.1088/1748-9326/4/4/044013.
- 57. M. Pósfai, A. Gelencsér, R. Simonics, K. Arató, J. Li, P. V. Hobbs, P. R. Buseck, *J. Geophys. Res. Atmos.*, in press, doi:10.1029/2003JD004169.
- 58. L. A. Goldberger, L. G. Jahl, J. A. Thornton, R. C. Sullivan, N2O5 reactive uptake kinetics
 and chlorine activation on authentic biomass-burning aerosol. *Environ. Sci. Process. Impacts.* 21, 1684–1698 (2019).
- A. T. Ahern, L. Goldberger, L. Jahl, J. Thornton, R. C. Sullivan, Production of N2O5 and
 ClNO2 through Nocturnal Processing of Biomass-Burning Aerosol. *Environ. Sci. Technol.* 52, 550–559 (2018).
- 679 60. Q. Bian, S. H. Jathar, J. K. Kodros, K. C. Barsanti, L. E. Hatch, A. A. May, S. M. Kreidenweis, J. R. Pierce, Secondary organic aerosol formation in biomass-burning plumes: theoretical analysis of lab studies and ambient plumes. *Atmos. Chem. Phys.* **17**, 5459–5475 (2017).
- 683 61. N. G. A. Mahfouz, N. M. Donahue, Primary ion diffusion charging and particle wall loss in smog chamber experiments. *Aerosol Sci. Technol.* **54**, 1058–1069 (2020).
- T. B. Onasch, A. Trimborn, E. C. Fortner, J. T. Jayne, G. L. Kok, L. R. Williams, P.
 Davidovits, D. R. Worsnop, C. Hare, J. Olfert, J. R. Kimmel, D. Sueper, H. Coe, J. Allan, E.
 Cross, S. Ng, D. Liscinsky, B. Mcmanus, L. Gonzalez, Soot Particle Aerosol Mass
 Spectrometer: Development, Validation, and Initial Application. *Aerosol Sci. Technol.* 46, 804–817 (2012).
- 690 63. M. Polen, T. Brubaker, J. Somers, R. C. Sullivan, Cleaning up our water: Reducing 691 interferences from nonhomogeneous freezing of "pure" water in droplet freezing 692 assays of ice-nucleating particles. *Atmos. Meas. Tech.* **11**, 5315–5334 (2018).

- 693 64. G. Vali, Quantitative Evaluation of Experimental Results and the Heterogeneous 694 Freezing Nucleation of Supercooled Liquids. *J. Atmos. Sci.* **28**, 402–409 (1971).
- 695 65. G. Vali, Revisiting the differential freezing nucleus spectra derived from drop-freezing experiments: methods of calculation, applications, and confidence limits. *Atmos.* 697 *Meas. Tech.* **12**, 1219–1231 (2019).
- 698 66. M. Polen, E. Lawlis, R. C. Sullivan, The unstable ice nucleation properties of Snomax bacterial particles. *J. Geophys. Res. Atmos.* **121**, 11666–11678 (2016).
- 700 67. A. D. Maynard, Estimating Aerosol Surface Area from Number and Mass Concentration Measurements. *Ann. occup. Hyg.* **47**, 123–144 (2003).
- 68. G. Buonanno, M. Dell'Isola, L. Stabile, A. Viola, Uncertainty budget of the SMPS-APS system in the measurement of PM1, PM2.5, and PM10. *Aerosol Sci. Technol.* **43**, 1130–1141 (2009).

Acknowledgements

705

706

707 **General:** For assisting with electron microscopy analysis, we thank Libor Kovarik, Swarup 708 China, and the staff at the Environmental and Molecular Sciences Laboratory at Pacific Northwest National Laboratory. For providing us with authentic biomass fuels we thank: 709 Stacy Freitas at the Klamath Basin National Wildlife Refuge Complex, Stephen Enloe at the 710 University of Florida UF/IFAS Center for Aqueous and Invasive Plants, Jonathan Glueckert at 711 the Loxahatchee National Wildlife Refuge, and Bert Wyatt at the Savannah National Wildlife 712 Refuge. Funding: This work was supported by the National Science Foundation (CHE-713 714 1554941; AGS-1552608; CBET-1804737); an NSF Graduate Research Fellowship for MP; L. Jahl and BB were partially supported by Steinbrenner Fellowships from CMU; TB was partially 715 supported by collaborative student grant from the Department of Mechanical Engineering 716 717 at CMU. Author Contributions: Conceptualization: RS; Investigation: L. Jahl, TB, MP, L. Jahn, KPC, BB, SG, RS; Formal Analysis: L. Jahl, TB, MP, L. Jahn, KPC, WF, RS; Writing: L. Jahl, RS. 718 Competing Interests: The authors declare no competing interests. Data and materials 719 availability: Data used to produce the presented results will be made available in the 720 721 ICARUS database for aerosol chamber experiments.

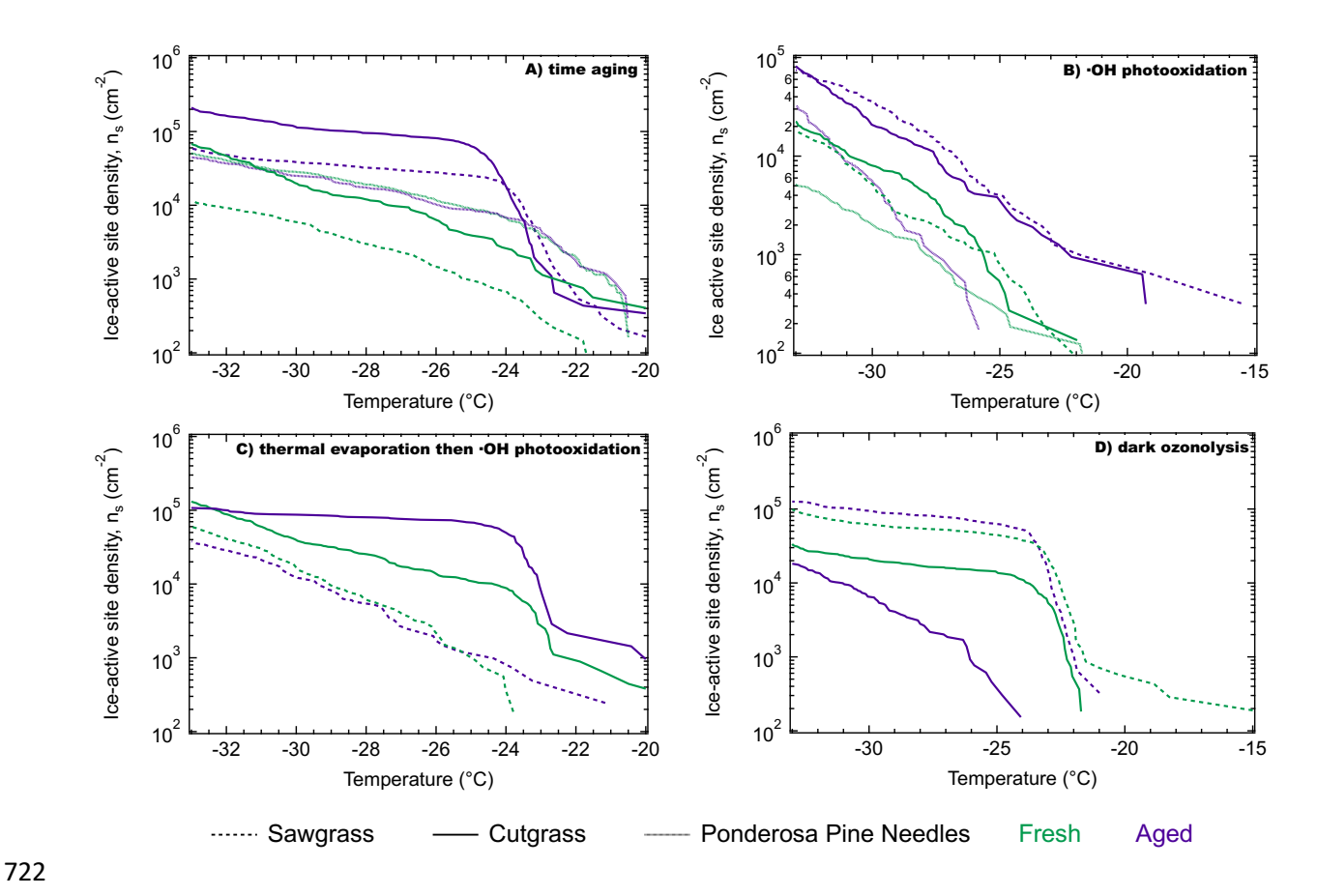


Figure 1. Ice-active surface site density (*n*_s) **plotted versus freezing temperature.** Each panel shows one type of aging of biomass-burning aerosol produced from combustion of cutgrass, sawgrass, or ponderosa pine. Fresh samples (prior to external perturbation or time aging) are shown in green and aged samples following several hours of chamber aging are shown in purple. **A)** time aging experiments revealed substantial increases in INA along with evaporation of organic carbon aerosol; **B)** hydroxyl radical photooxidative aging caused slight increases in INA (additional experiments shown in Fig. S2); **C)** thermal evaporation of the BBA followed by hydroxyl radical photooxidation revealed mixed effects on INA; and **D)** ozonolysis without photochemistry resulted in no observed changes or a prominent decrease in INA in one case, along with substantial increases in the organic aerosol mass loading. A subset of these experiments shown with 95% confidence intervals is provided in Figure S3 in the Supplementary Materials, and the ice-active site density normalized to the mass concentration of black carbon aerosol (a conserved non-volatile tracer) rather than aerosol surface area is provided in Figure S9.

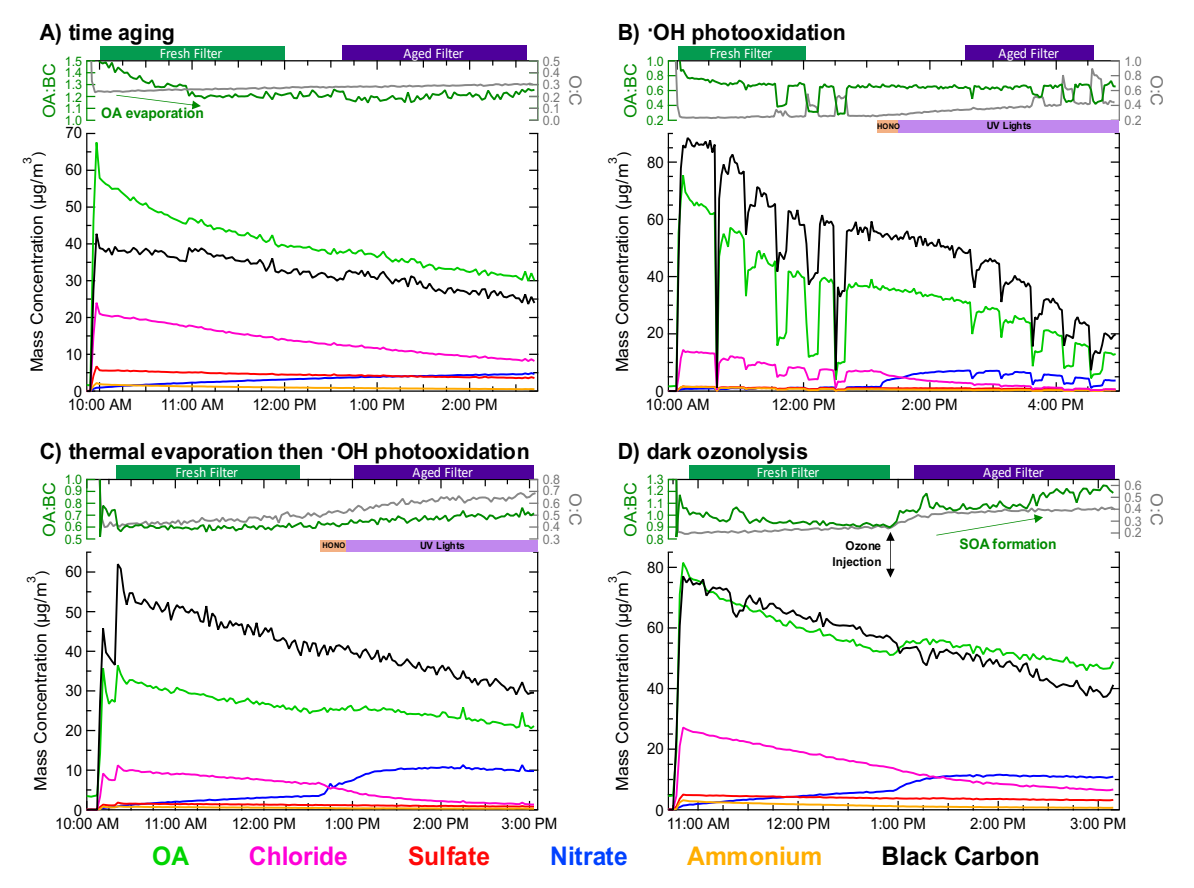


Figure 2. Exemplary evolution of submicron aerosol chemical composition in the four types of simulated atmospheric aging explored. Each panel shows SP-AMS chemical composition measured for one type of aging. Mass concentration (trace color corresponds to chemical component) in SP-mode is plotted in the lower portion; the organic aerosol:black carbon ratio – a measure of the gain or loss of OA versus the conserved BC tracer that only undergoes chamber wall loss - is plotted on the upper left axis. A measure of OA oxidation state, the O:C atomic ratio from El-mode measurements, is plotted on the upper right axis. OA:BC and O:C are unreliable during the first few minutes of experiment while the chamber is filling. Collection times of fresh and aged filters for INP analysis are shown by green and purple bars, respectively, on the top of each panel. A) Cutgrass time aging experiment with considerable evaporation of organic aerosol observed in the OA:BC ratio. B) Sawgrass photooxidation experiment; HONO injection is shown by the orange bar and UV illumination by the purple bar. Sudden decreasing mass concentration and increasing O:C occurred when the aerosol particles were passed through a heated thermodenuder before entering the SP-AMS. C) Sawgrass experiment where the BBA was subjected to thermal desorption at 250 °C before injection into chamber. HONO injection is shown by the orange bar and UV illumination by the purple bar. D) Cutgrass dark ozonolysis experiment, with 350 ppb of ozone injected at the labeled time. The formation of SOA is indicated through the increase in OA:BC following ozone injection.

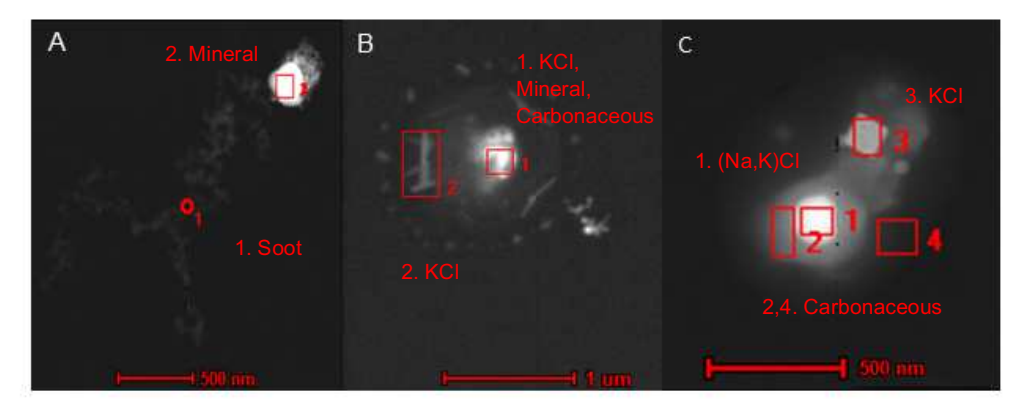


Figure 3. Transmission electron microscopy (TEM) images of fresh BBA. A-B) are from ponderosa pine needles and **C)** is from sawgrass BBA collected on substrates indicating the presence of organic aerosol coatings around mineral-containing particles. Particle **A** is a fractal soot particle agglomerated with an iron-based mineral in the region indicated by the box. Particle **B** has a mixed core in region 1 composed of KCI, minerals, and carbonaceous material, with additional KCI in region 2 and a carbonaceous OA coating that appears gray surrounding the entire particle. Particle **C** contains several inorganic salt phases in regions 1 & 3 and is also surrounded by an OA coating that appears gray in regions 2 & 4. EDX spectra of the boxed regions are provided in Fig. S6.

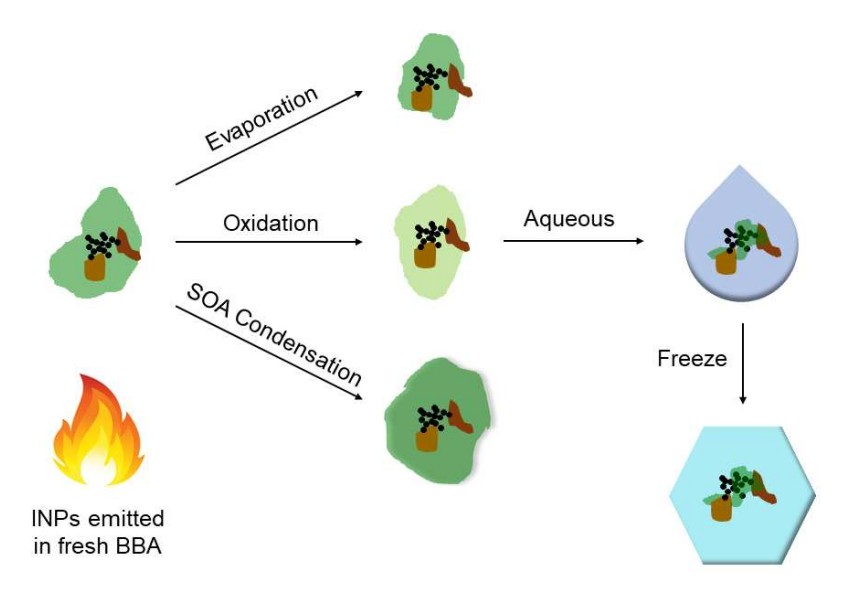


Figure 4. Schematic representation of the atmospheric co-evolution BBA composition and ice-nucleation activity. The particle contains minerals depicted in shades of brown, soot depicted in black, and organic aerosol depicted in green. Evaporation of OA leads to increased availability of ice-active sites. Oxidation of OA changes its chemical composition to be more oxidized and water-soluble organic carbon such that when the particle is immersed in a droplet the OA can dissolve more readily to reveal ice-active sites. Secondary organic aerosol (SOA) condensation from oxidation and condensation of organic carbon onto the particle conceals ice-active sites. This schematic represents the different biomass-burning aerosol aging processes that may occur in the atmosphere, which are not ordinarily decoupled as depicted and can occur simultaneously or in competition to varying degrees.

Supplementary Materials

Summary

Below we show six additional figures to support our findings presented in the main manuscript. Figure S1 shows the experimental setup of the chamber used for authentic biomass-burning aerosol (BBA) aging experiments. Figure S2 shows additional ice-active site density (n_s) vs. temperature spectra for fresh and aged BBA through ·OH photooxidation not depicted in Figure 1 to prevent overcrowding the main figure. As discussed in the main paper, all of these samples had an increase in INA with photooxidative aging across at least some temperature ranges.

Figure S3 shows selected ice-active site density (n_s) vs. temperature spectra with 95% confidence intervals, demonstrating which aging experiments exhibited statistically significant changes between the INA of fresh versus aged BBA. Shaded 95% confidence intervals shown were calculated following the Monte Carlo method presented by Vali (65). Briefly, each freezing experiment was discretized into 0.25 °C temperature bins. Then μ , the number of droplets that freeze in each temperature bin, can be approximated as a Poisson process and the random spread of μ approaches a Poisson distribution. A series of 100 outcomes are drawn from each Poisson distribution to produce 100 simulated experiments, each with a new n_s spectrum. The linearly interpolated 2.50% and 97.5% quantiles of n_s at each discrete temperature are then interpreted as the 95% confidence intervals (p = 0.05).

Figure S4 shows the raw frozen fraction temperature spectra (rather than n_s plots, because all droplets froze within the filtered water background freezing temperature range) for two wood BBA samples. This demonstrates that photooxidative aging does not increase the INA of BBA produced from wood combustion, which tends to produce fewer mineral particles and more soot compared to the tall grass fuels. Figure S5 shows the mass fraction of organic aerosol remaining after passing through a heated thermodenuder - used to determine the volatility of the fresh and aged BBA. Figure S6 shows TEM/EDX spectra of the BBA particles depicted in Figure 3, used to determine the chemical composition of different regions of individual particles. Many particles have organic aerosol coatings which evaporate to reveal ice-active sites, leading to an increase in INA for aged BBA. Figure S7 shows frozen fraction temperature spectra of filtered water and filter handling blank samples, and includes a discussion of errors inherent to the INA analysis and surface area measurements. Figure S8 shows two example averaged surface area distributions from fresh and aged aerosol populations. Figure S9 shows the INA normalized to black carbon mass concentration rather than particle surface area; the trends in INA with aging are consistent to those observed in the n_s spectra discussed in the main text.

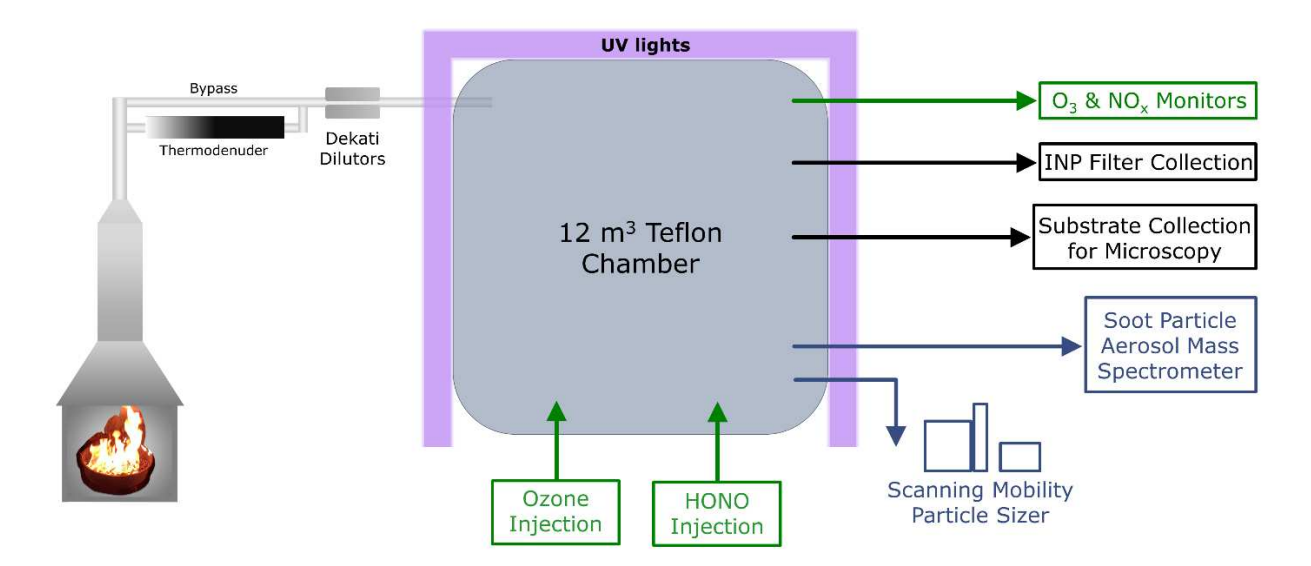


Figure S1. Experimental setup for chamber aging of authentic BBA. Experiments were conducted in the combustion facility of the CMU Air Quality Laboratory. Each fuel was burned in a galvanized steel pan inside a partial enclosure. Clean air diluted and pulled the resulting smoke into a $12~\text{m}^3$ Teflon chamber which was thoroughly flushed overnight with clean air and UV radiation before each experiment. For experiments with BBA passed through the thermodenuder before chamber injection, the Dekati dilutors were operated at a lower flowrate to increase the residence time of the aerosol in the thermodenuder. Ozone was produced from pure $O_2(g)$ using a corona discharge ozone generator and nitrous acid (HONO) vapor was produced from the headspace of a solution of sodium nitrite and sulfuric acid.

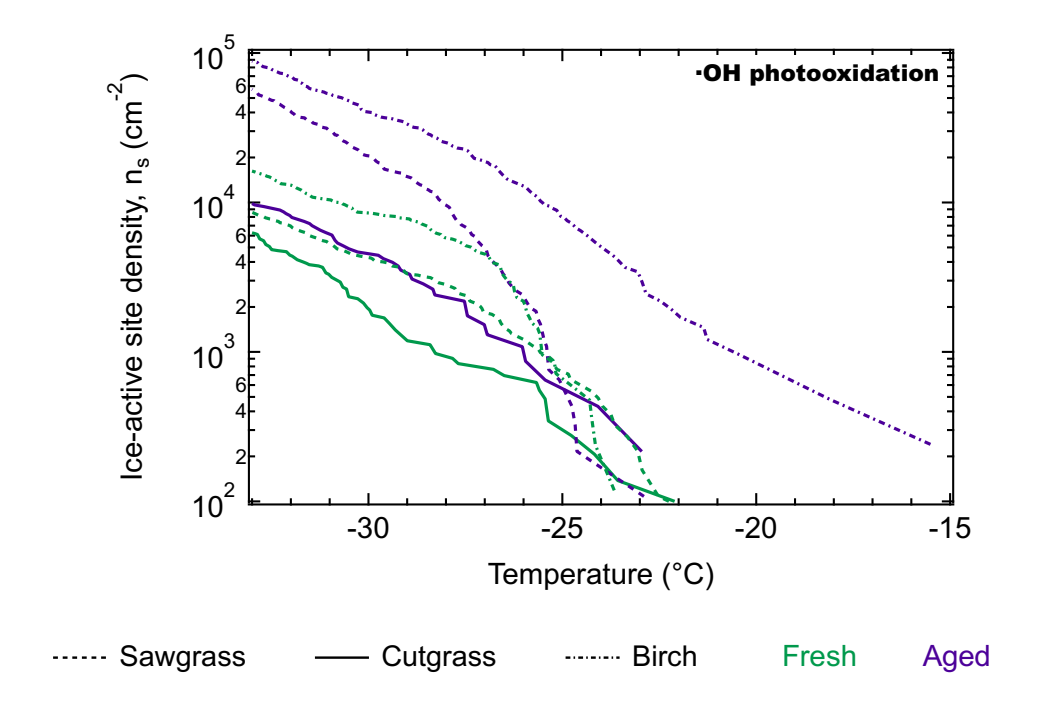


Figure S2. Ice-active surface site density (*n*_s) **temperature spectra for additional BBA 'OH photooxidation aging experiments.** The experiments here are 'OH photooxidation of biomass-burning aerosol produced from combustion of cutgrass, sawgrass, or birch. Fresh BBA samples (prior to external perturbation) are shown in green and aged samples following several hours of chamber photooxidative aging are shown in purple. 'OH photooxidation tended to increase the INA across most if not all temperatures, similar to the results shown in Figure 1. The birch experiment shown here was the only BBA produced from wood (as opposed to grass) combustion that showed appreciable INA and an increase in INA after aging. See Fig. S4 for additional data and discussion on wood BBA.

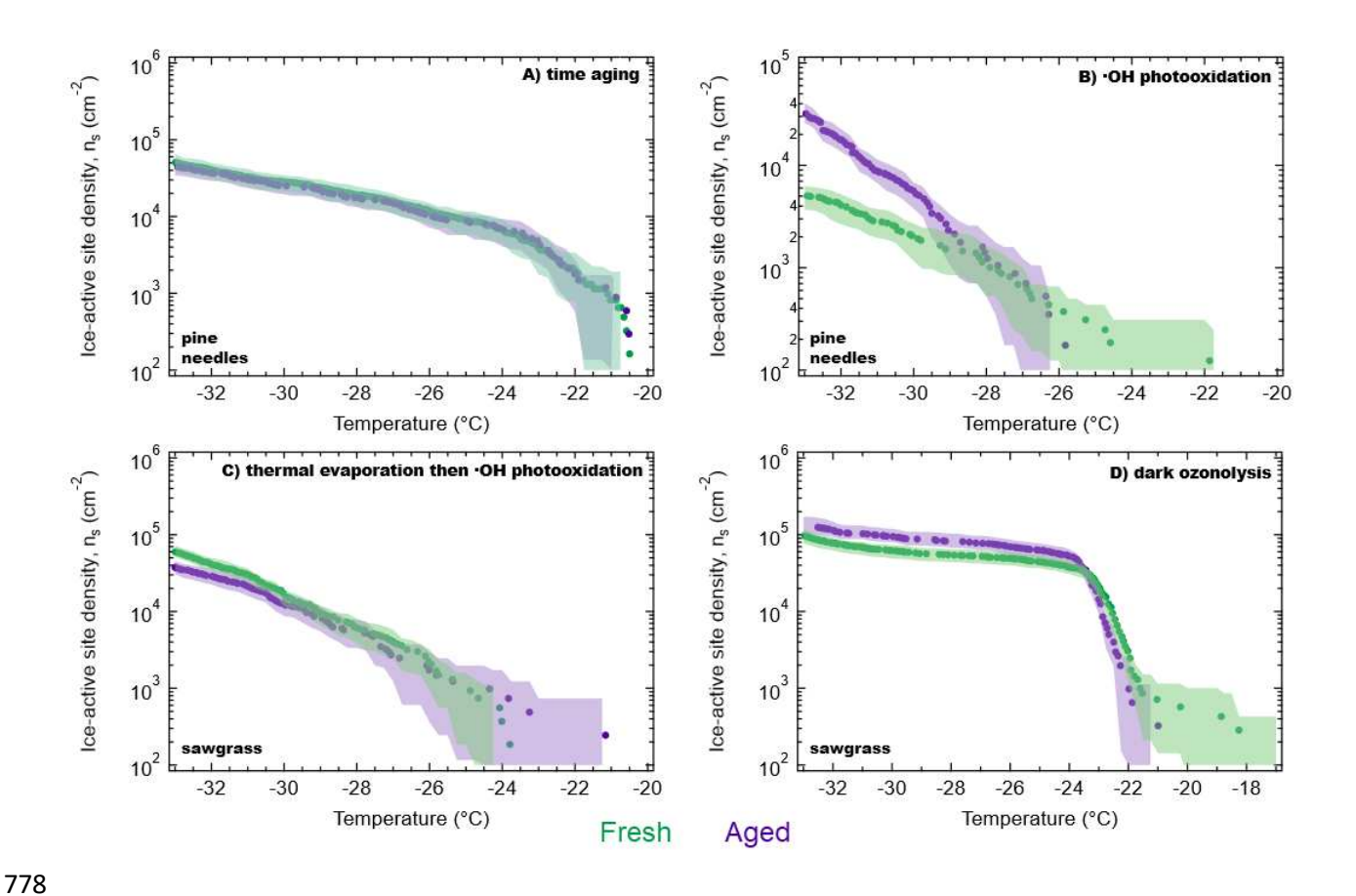


Figure S3. Selected n_s spectra from Figure 1 with 95% confidence intervals shown. One experiment for each aging type (fuel indicated within each panel) was chosen based off their fresh and aged ice-active site densities being the most similar. Shaded 95% confidence intervals were calculated following the Monte Carlo method presented by Vali (60) as described above. This emphasizes that unless the INA of the fresh and aged are extremely similar, we can confidently state that the observed increases in INA are statistically significant and beyond measurement uncertainty or variability. For A) time aging here there is no significant difference between fresh and aged, but in all other experiments in Fig.1, the fresh and aged BBA are significantly different at temperatures < -23.5 °C. For B) OH photooxidation experiments, the aged ponderosa pine needle BBA is significantly greater than the fresh BBA only at temperatures < -29.6 °C, while the fresh & aged cutgrass and sawgrass experiments in Fig. 1 are different < -27.2 °C and < -24.2 °C, respectively. The C) thermal evaporation then OH photooxidation sawgrass experiment shown here does not have a statistically significant difference between the fresh and aged aerosol, but for the cutgrass experiment in Fig. 1, fresh and aged BBA are different between -23 °C and -31 °C. The D) dark ozonolysis sawgrass experiment has no significant difference between fresh and aged BBA, while the cutgrass experiment in Fig. 1 has a significant decrease in INA after aging across all temperatures. These data show that at temperatures relevant to mixed-phased clouds, there are statistically significant increases in INA after dilution, evaporation, and photooxidative aging, and no increase or even a statistically significant decrease in INA following aging that involved substantial SOA production.

780

781

782

783

784 785

786 787

788

789 790

791

792

793 794

795

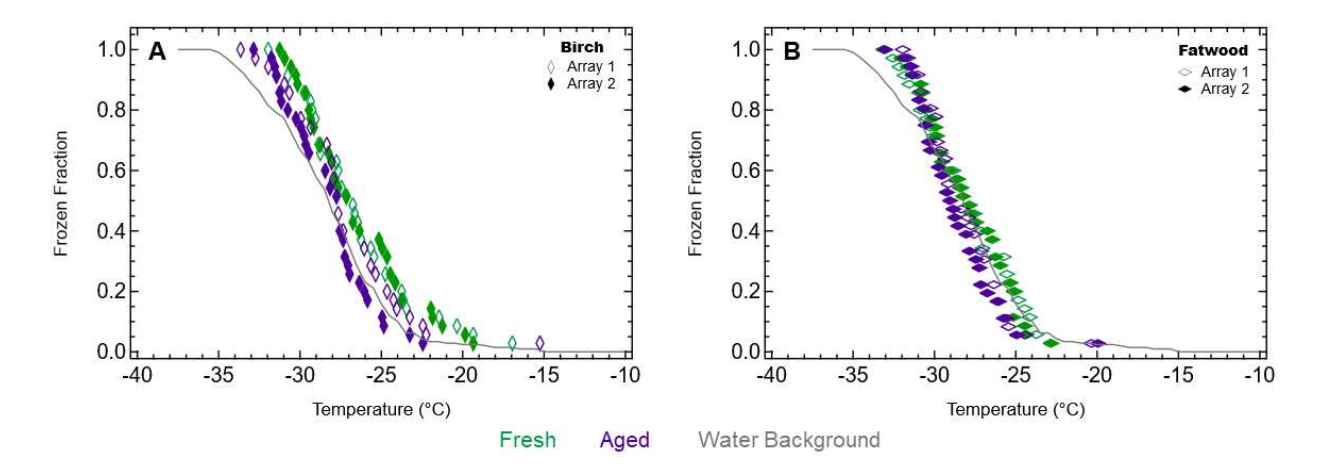


Figure S4. Frozen fraction temperature spectra for BBA from two wood fuels. Ice nucleation analysis was performed by a traditional droplet-on-substrate technique; method details are described by Polen et al. (63, 66). BBA from birch wood (A) and fatwood (B) was subjected to ·OH photooxidation without additional NO_x, and no increase in INA was observed. Average background freezing temperature spectrum for filtered water shown as gray line; all BBA sample data for birch and fatwood lay within the water background freezing spectrum. Based off of previous work, EDX revealed less mineral formation in BBA produced from woods compared to tall grasses, with slightly more minerals present in birch BBA compared to fatwood BBA (26). The combustion of these woods also produced the most black carbon (BC) in the aerosol compared to other fuels studied – birch BBA was 65% BC by mass and fatwood was 86% BC as measured by the SP-AMS. The reasoning behind the lack of increase in INA with aging observed here is consistent with our previous discussion. For wood fuels, there are few mineral-based ice-active sites present in even the fresh BBA, so any evaporation of organic carbon coatings – that revealed the mineral-based ice-active sites in BBA produced from grass combustion – made no difference in the INA of aged BBA produced from the combustion of these woods. These results further emphasize that black carbon from biomass combustion cannot explain the ice activity of BBA, or how it responds to aging.

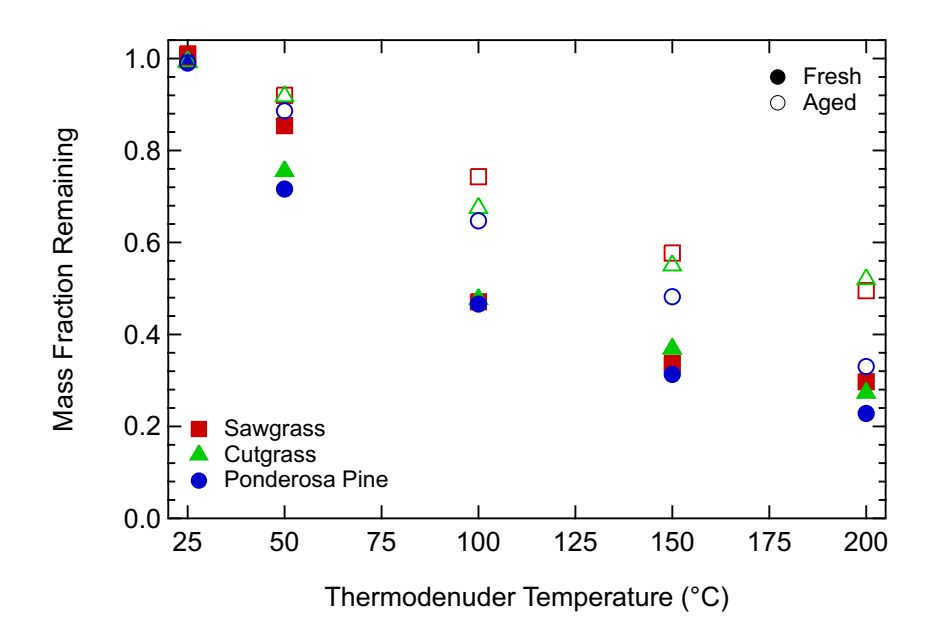


Figure S5. Effects of ·OH photooxidative aging on the volatility of organic aerosol (OA) in BBA. Trends in aerosol volatility are demonstrated based on the mass fraction of OA remaining after being subjected to thermal desorption, plotted as a function of thermodenuder (TD) temperature. The OA mass fraction remaining was calculated from the SP-AMS in laser-off mode by dividing the OA concentration following the TD by the OA concentration following an unheated bypass line. Filled symbols indicate fresh BBA, while hollow symbols indicate ·OH-aged BBA. For each of these fuels, the mass fraction remaining after aging is less than that for the fresh aerosol particles, indicating that aged aerosol is less volatile. This complements our understanding of how organic aerosol aging reveals ice-active sites present in the BBA. The TD methodology used here is further described by Cain & Pandis (35). All SP-AMS data analysis was completed in the Igor software packages SQUIRREL (version 1.62A) and PIKA (version 1.22A).

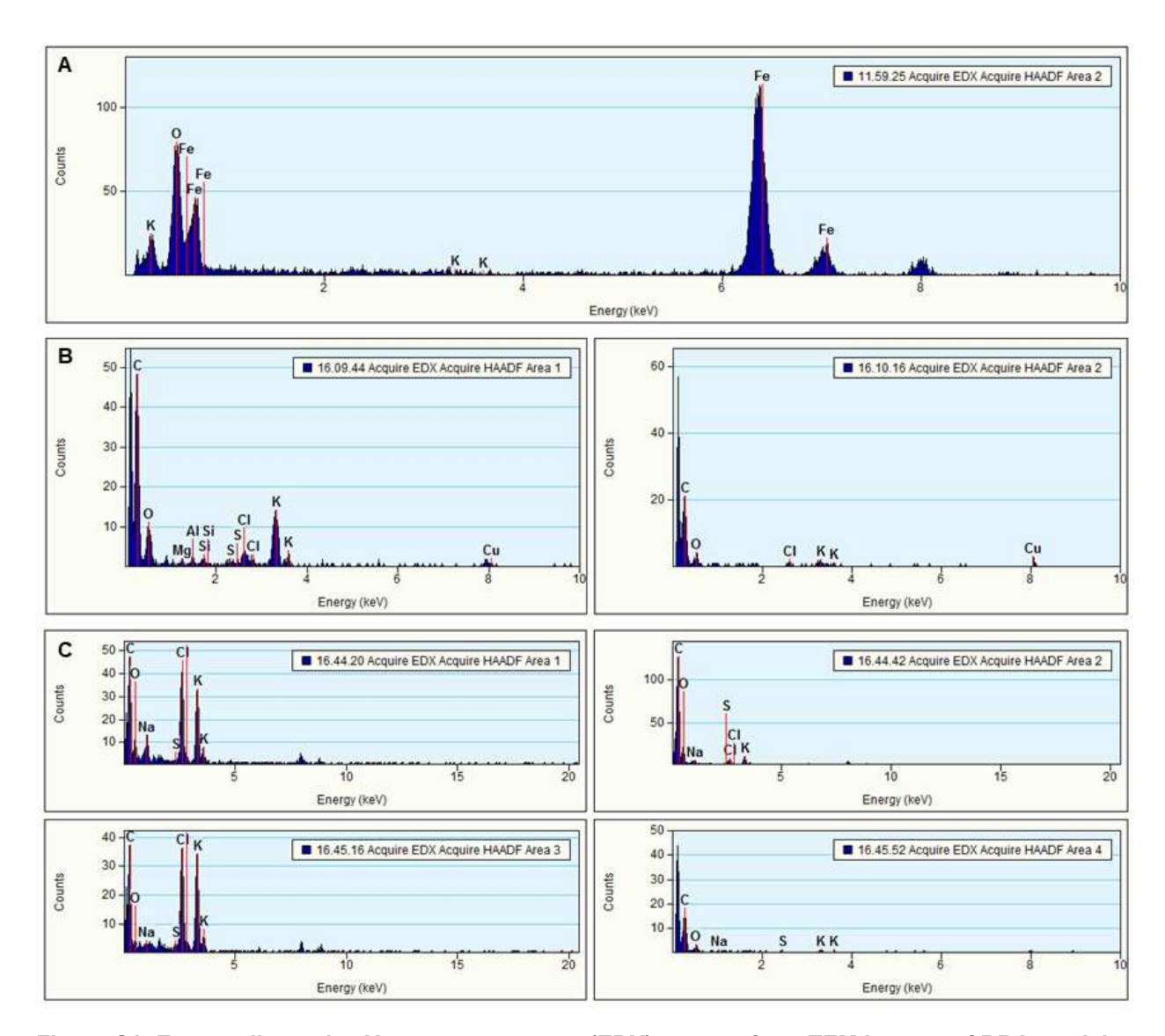


Figure S6. Energy dispersive X-ray spectroscopy (EDX) spectra from TEM images of BBA particles displayed in Figure 3. The ordering of the particle microscopy images and spectra here are the same as in Figure 3, and the area numbers within the legend of each spectrum here corresponds to the numbered regions in Fig. 3. Particle **A)** EDX spectrum shows the iron-based mineral region. Particle **B)** EDX spectra show region 1 composed of KCI; AI, Mg, and Si-containing minerals; and carbonaceous material, with additional KCI in region 2. Particle **C)** EDX spectra show chloride salts in regions 1 & 3, and carbonaceous material in regions 2 & 4 on the outer edges of the particle. These spectra, as well as previous work on the same biomass fuels, show organic aerosol coating inorganic/mineral regions, supporting our new framework suggesting that OA evaporation exposes the ice-active mineral surface sites in BBA (26).

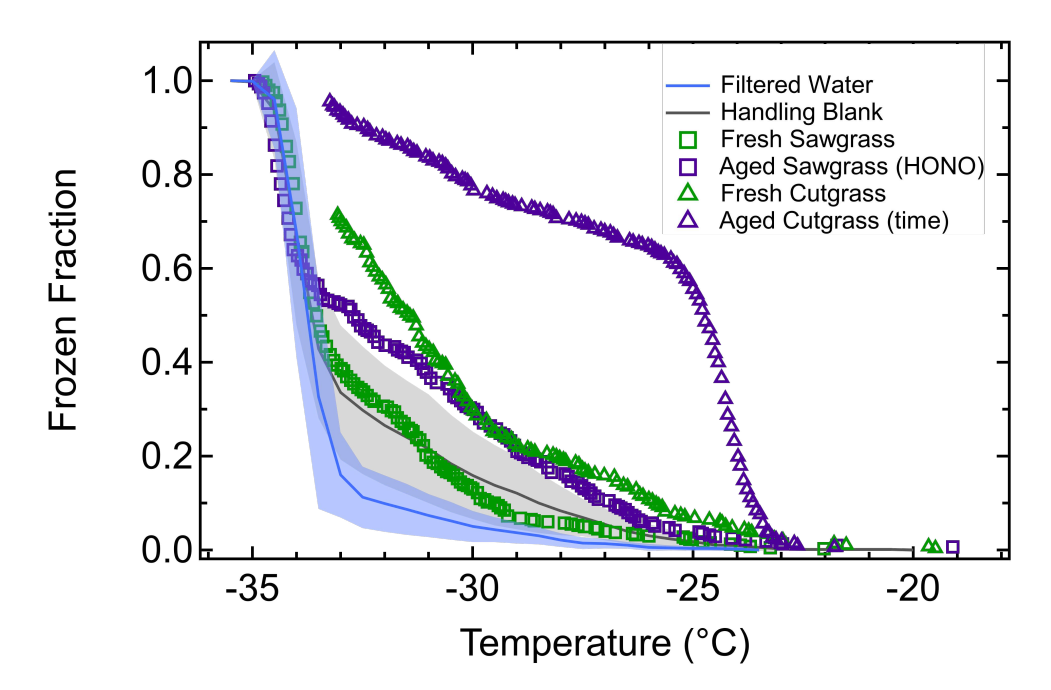


Figure S7. Frozen fraction temperature spectra for filtered water, handling blank, and representative BBA samples. Freezing temperature observed for 6 nL droplets using the store-and-create microfluidic device during a 1 °C/min cooling cycle. The blue line and shaded area are the average and standard deviation of nine runs of droplets generated from filtered water. The filtered water background freezing spectrum plotted here is identical to the filtered water curves shown in Polen et al. (2018) and Brubaker et al. (2020) since they were completed throughout the analysis time period of the many BBA samples. The gray line and shaded area are the average and standard deviation of nine runs of filter extracts collected as handling blanks (processed exactly the same as BBA filter samples except there was no BBA-laden airstream sampled across the filters). Two experiments - a sawgrass HONO aging experiment and a cutgrass time aging experiment – are shown for a comparison to the filtered water and handling blank frozen fraction spectra. The filtered water background freezing occurred well below the droplet freezing temperature observed of the BBA samples, and handling filter blanks were only slightly higher than filtered water background freezing, still much lower than most BBA samples. The only samples that were within the background levels of the handling blank were the fresh sawgrass sample shown here, the fresh ponderosa pine needle sample in Fig. 1B, and the aged cutgrass sample in Fig. 1D. Notably, the corresponding fresh/aged BBA samples for each of these three samples are all above the handling blank values, validating the trends in INA with aging discussed in the paper.

Uncertainties in ice-active site density temperature spectra (n_s) from background freezing, filter handling blanks, and aerosol size distribution measurements

The temperature uncertainties for the measured droplet freezing temperatures is ± 0.2 °C (32), and droplets that are smaller than the standard volume of 6 nL are not used in analysis as these droplets would contain a different amount of INPs and bias our results. Some droplets within the microfluidic device are not counted by the droplet detection program (depending on specific lighting in the laboratory at the time of analysis), but this is less than 2% of the total droplets. Considering both of these factors, about 500 6 nL droplets are still analyzed per sample, producing a high-resolution frozen fraction temperature spectrum from which n_s is derived.

We use the average aerosol size distribution from SMPS measurements and the total surface area estimated from this to calculate n_s for each experiment, fresh or aged, thus accounting for changes in the aerosol surface area during an experiment from the fresh to aged period. The SMPS measured particles up to 750 nm in mobility diameter, and while the total surface area decreased throughout the experiments by about 40%, with the geometric mean diameter increasing by about 10%, less than 1% of particles had a mobility diameter greater than 500 nm even at the end of each experiment. Example averaged surface area distributions from fresh and aged aerosol populations are shown in Fig. S8. Considering the small amount of the particle surface area collected onto filters for ice nucleation analysis but not measured by the SMPS of ~1%, n_s values are biased slightly high but similarly for both the fresh and aged samples. Uncertainty in the aerosol aerodynamic diameter is about 20%, and at maximum, SMPS surface area estimates have an error of four times the actual value (67, 68). Since n_s scales linearly with surface area, the surface area would have to have error of an order of magnitude to cause an apparent increase in n_s of an order of magnitude.

Additionally, while there can be some differences in particle morphology between the fresh and aged BBA samples, the relative error in surface area determination between fresh and aged would be much less than any absolute error in surface area. Therefore, comparing INA through n_s values as we have corrects for most systematic errors in the estimated surface area since we are comparing two n_s spectra obtained from the same chamber experiment and the same measurement methods. Determination of particle surface area through microscopy was not employed as the apparent particle size can change when particles are impacted on the substrate or exposed to the TEM vacuum chamber and it is extremely logistically difficult to image enough particles at high enough resolution to accurately quantify particle surface area. We do not report ice-nucleating activity as n_m (normalized to aerosol mass) since estimating mass from the SMPS size distribution is just as if not more uncertain than estimating surface area, and weighing aerosol filter samples to determine the total mass and would also have significant uncertainty given the total aerosol mass present in the chamber. However, to confirm that the observed trends in INA were not due to errors in surface area estimation or artifacts in how the surface area distributions changed over time, the INA can be plotted normalized to the mass of black carbon in the BBA, shown below in Fig. S9.

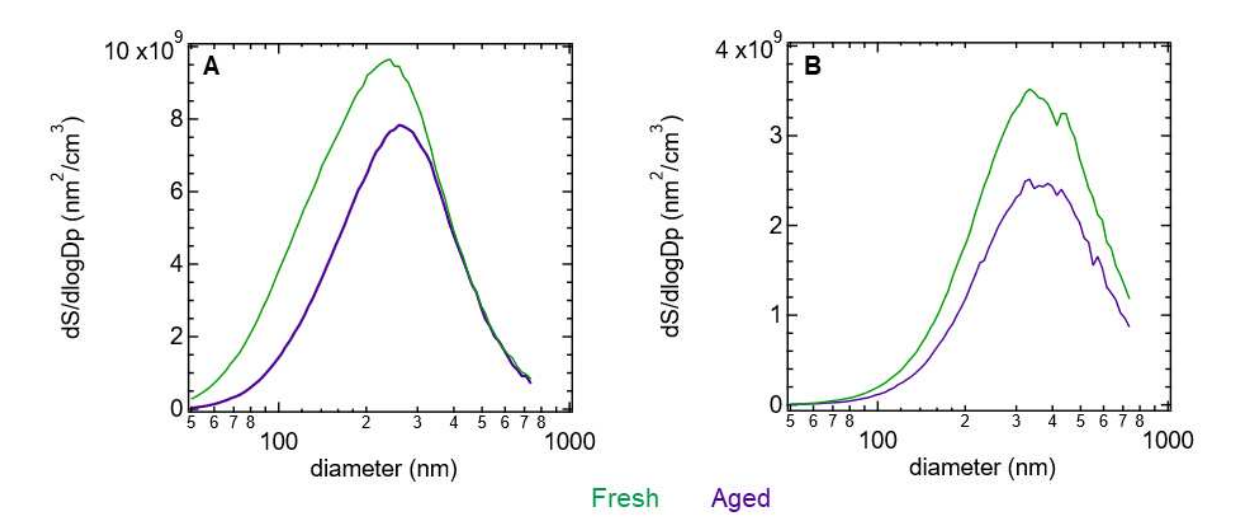


Figure S8. Average surface area distributions from fresh (green) and aged (purple) aerosol populations for a cutgrass time aging experiment (A) and cutgrass 'OH photooxidation experiment (B). The total surface area decreases throughout the experiments and how the aerosol size distribution changes across time varies slightly between different experiments, but these changes are minimal and are accounted for when normalizing the INA by black carbon, as shown in Fig. S9. Therefore, these changes in surface area distributions do not affect our conclusions.

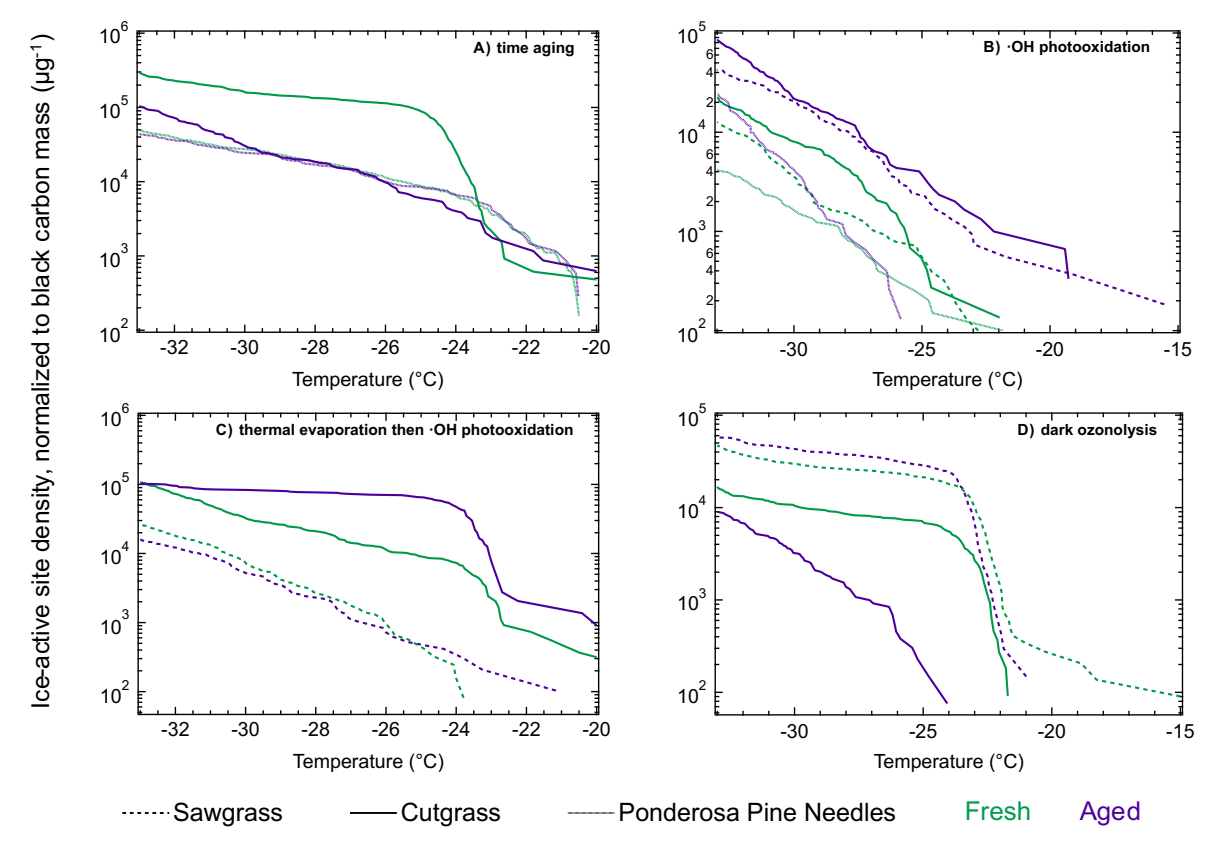


Figure S9. Ice-active site density of the BBA aging experiments shown in Fig. 1, normalized to the aerosol mass concentration of black carbon rather than total particle surface area. There are only slight differences between the spectra shown here normalized to black carbon (a conserved non-volatile aerosol tracer) and those in Figure 1 normalized to the SMPS-measured aerosol surface area. This indicates that the trends in INA with aging are real effects and not simply caused by changes in the total surface area measured by the SMPS. Black carbon mass concentration was determined by the SP-AMS and was averaged across the collection time of each fresh or aged filter. The sawgrass experiment in Figure 1 panel A is not shown here as an SP-AMS failure occurred halfway through this experiment, preventing measurements of black carbon.